

# Evaluation of Daytime Measurements of Aerosols and Water Vapor made by an Operational Raman Lidar over the Southern Great Plains

Richard Ferrare<sup>1</sup>, David Turner<sup>2</sup>, Marian Clayton<sup>3</sup>, Beat Schmid<sup>4</sup>, Jens Redemann<sup>4</sup>,  
David Covert<sup>5</sup>, Robert Elleman<sup>5</sup>, John Ogren<sup>6</sup>, Elisabeth Andrews<sup>6</sup>,  
John E.M.Goldsmith<sup>7</sup>, Haflidi Jonsson<sup>8</sup>

February 3, 2005

Submitted to Journal of Geophysical Research – Atmospheres  
DOE ARM May 2003 Aerosol IOP Special Section

---

<sup>1</sup> NASA Langley Research Center, MS 401A, Hampton, VA, 23681, USA, [richard.a.ferrare@nasa.gov](mailto:richard.a.ferrare@nasa.gov)

<sup>2</sup> Pacific Northwest National Laboratory, P.O. Box 999/K9-24, Richland, WA, 99352, US, [dave.turner@pnl.gov](mailto:dave.turner@pnl.gov)

<sup>3</sup> SAIC/NASA Langley Research Center, MS 401A, Hampton, VA, 23681, USA, [m.b.clayton@larc.nasa.gov](mailto:m.b.clayton@larc.nasa.gov)

<sup>4</sup> BAER Institute/NASA Ames Research Center, MS 245-5, Moffett Field, CA, 94035, USA,  
[bschmid@mail.arc.nasa.gov](mailto:bschmid@mail.arc.nasa.gov), [jredemann@mail.arc.nasa.gov](mailto:jredemann@mail.arc.nasa.gov)

<sup>5</sup> Dept. of Atmospheric Sciences, Univ. of Washington, Box 351640, Seattle, WA, 98195, USA,  
[dcovert@u.washington.edu](mailto:dcovert@u.washington.edu), [rob@atmos.washington.edu](mailto:rob@atmos.washington.edu)

<sup>6</sup> NOAA/CMDL, 325 Broadway R/CMDL1, Boulder, CO, 80305, USA, [John.A.Ogren@noaa.gov](mailto:John.A.Ogren@noaa.gov),  
[Betsy.Andrews@noaa.gov](mailto:Betsy.Andrews@noaa.gov)

<sup>7</sup> Sandia National Laboratories, P.O. Box 969, Livermore, CA, 94551-0969, USA, [jgold@sandia.gov](mailto:jgold@sandia.gov)

<sup>8</sup> CIRPAS/Naval Postgraduate School, 3240 Imjin Road, Marina, CA 93933, USA, [hjonsson@nps.navy.mil](mailto:hjonsson@nps.navy.mil)

## Abstract

Raman lidar water vapor and aerosol extinction profiles acquired during the daytime over the Department of Energy (DOE) Atmospheric Radiation Measurement (ARM) Southern Great Plains (SGP) site in northern Oklahoma (36.606 N, 97.50 W, 315 m) are evaluated using profiles measured by *in situ* and remote sensing instruments deployed during the May 2003 Aerosol Intensive Operations Period (IOP). The automated algorithms used to derive these profiles from the Raman lidar data were first modified to reduce the adverse effects associated with a general loss of sensitivity of the Raman lidar since early 2002. The Raman lidar water vapor measurements, which are calibrated to match precipitable water vapor (PWV) derived from coincident microwave radiometer (MWR) measurements were, on average, 5-10% ( $0.3\text{-}0.6\text{ g/m}^3$ ) higher than the other measurements. Some of this difference is due to out-of-date line parameters that were subsequently updated in the MWR PWV retrievals. The Raman lidar aerosol extinction measurements were, on average, about  $0.03\text{ km}^{-1}$  higher than aerosol measurements derived from airborne Sun photometer measurements of aerosol optical thickness and *in situ* measurements of aerosol scattering and absorption. This bias, which was about 50% of the mean aerosol extinction measured during this IOP, decreased to about 10% when aerosol extinction comparisons were restricted to aerosol extinction values larger than  $0.15\text{ km}^{-1}$ . The lidar measurements of the aerosol extinction/backscatter ratio and airborne Sun photometer measurements of the aerosol optical thickness were used along with *in situ* measurements of the aerosol size distribution to retrieve estimates of the aerosol single scattering albedo ( $\omega_0$ ) and the effective complex refractive index. Retrieved values of  $\omega_0$  ranged from (0.91-0.98) and were in generally good agreement with  $\omega_0$  derived from airborne *in situ* measurements of scattering and absorption. Elevated aerosol layers located between about 2.6 and 3.6 km were observed by the Raman lidar on May 25 and May 27. The airborne measurements and lidar retrievals indicated that these layers, which were likely smoke produced by Siberian forest fires, were primarily composed of relatively large particles ( $r_{\text{eff}} \sim 0.23\text{ }\mu\text{m}$ ), and that the layers were relatively non-absorbing ( $\omega_0 \sim 0.96\text{-}0.98$ ). Preliminary results show that major modifications that were made to the Raman lidar system during 2004 have dramatically improved the sensitivity in the aerosol and water vapor channels and reduced random errors in the aerosol scattering ratio and water vapor retrievals by an order of magnitude.

## 1. Introduction

Measurements of water vapor and aerosol optical properties are required to meet two of the primary objectives of the Department of Energy Atmospheric Radiation Measurements (ARM) program, which are: 1) relate observations of radiative fluxes and radiances to the atmospheric composition and, 2) use these relations to develop and test parameterizations to accurately predict the atmospheric radiative properties. Measurements of water vapor are especially important for characterizing the atmospheric state because uncertainties in the water vapor field dominate the spectral effects in the atmospheric window region of  $800\text{-}1200\text{ cm}^{-1}$  ( $8.3\text{-}12.5\text{ }\mu\text{m}$ ) [DOE, 1990]. Vertical profiles of aerosol properties are key parameters required for determining how aerosols impact clouds [Feingold *et al.*, 1999] as well as for computing radiative flux profiles [Ruggaber *et al.*, 1994; Wendisch *et al.*, 1996; Charlock and Alberta, 1996] and aerosol radiative forcing [Haywood and Ramaswamy, 1998]. Direct radiative forcing is very sensitive to aerosol absorption, commonly expressed in terms of the aerosol single scattering albedo  $\omega_0$ , so that an error of a few percent in  $\omega_0$  can make a difference between tropospheric heating or cooling for a given surface albedo [Russell *et al.*, 2002].

Because of the importance of water vapor and aerosols, ARM has aggressively pursued new technologies for systematic and routine measurements of water vapor and aerosols at the ARM Southern Great Plains (SGP) Climate Research Facility (CRF) site in northern Oklahoma (36.606 N, 97.50 W, 315 m). Such measurements are required to satisfy one of the goals of the ARM program, which is to collect a 10-yr dataset that can be used to study, and hence improve, the treatment of radiative transfer in the atmosphere, especially with respect to water vapor, aerosols, and clouds [Stokes and Schwartz, 1994]. One such example is the CRF Raman lidar (CARL), which operates as a turnkey, automated system for unattended, around-the-clock profiling of water vapor and aerosols [Goldsmith *et al.*, 1998]. This Raman lidar is unique in that it was designed for operations to remotely profile water vapor, aerosols, and clouds autonomously 24 hours per day, 7 days per week for several years.

Since this system is acquiring a unique data set that spans many years, it is important to periodically evaluate these measurements to ascertain how changes in instrument performance impact the retrieved data sets. ARM has attempted to characterize the water vapor measurement

performance of this instrument using routine intercomparisons and a series of water vapor Intensive Operation Periods (IOPs) [Revercomb *et al.* 2003; Ferrare *et al.*, 2004]. Results from these experiments show that when compared with water vapor measurements acquired by other ground and airborne remote sensors and *in situ* instruments, CARL water vapor measurements can serve as a stable transfer standard that requires only a single height-independent calibration factor. This calibration factor has typically been provided by comparing total integrated column water vapor with that provided by the ARM ground based Microwave Radiometer (MWR). However, these results have been based almost entirely on nighttime measurements, since CARL water vapor retrievals extend to near the tropopause (~10-12 km) [Goldsmith *et al.* 1998, Turner and Goldsmith 1999] at night, but have been limited to altitudes below about 3 km during the day. Previous, limited attempts to evaluate the CARL daytime water vapor measurement performance found significant (~10%) differences between the daytime and nighttime measurements [Turner and Goldsmith, 1999; Linne *et al.*, 2001]. Potential corrections to account for day-night differences in CARL operations have been developed, but the impacts of these corrections had not been examined through extensive intercomparisons.

Vertical profiles of aerosol properties are key parameters required for the computation of radiative flux profiles. ARM has supported the development of systematic and routine measurements of aerosols at the SGP CRF site, including measurements by surface *in situ* instruments [Sheridan *et al.*, 2001] as well as by CARL [Turner *et al.*, 2001] and periodic aircraft-borne *in situ* sensors [Andrews *et al.*, 2004] in the vertical column above the site, to try to obtain the relevant aerosol profile measurements required for these flux computations. However, initial comparisons of aerosol optical thickness and aerosol extinction, two of these key aerosol properties, have revealed discrepancies among the routine lidar, Sun photometer, and routine small aircraft *in situ* measurements [Ferrare *et al.*, 2002]. The May 2003 Aerosol Intensive Operations Period (IOP) was conducted in part to obtain more detailed measurements of aerosol optical properties to resolve these discrepancies, characterize the routine measurements of aerosol extinction profiles acquired by CARL, as well as to more completely characterize the aerosol optical, microphysical, and chemical properties at the surface and above the SGP site for accurately computing radiative fluxes. Consequently, in this study, we examine the ability of such a Raman lidar, when used in an *operational* mode several years after commencing

operations, to retrieve aerosol extinction and water vapor profiles during the daytime. This report represents the first such study that we are aware of. Another objective of the IOP was to measure aerosol optical properties (scattering, absorption, and extinction) using a number of different instruments simultaneously with measurements of direct and diffuse solar radiation in order to better understand and model the impact of aerosols on direct and diffuse radiation. Particular emphasis was placed on the role of aerosol absorption. Therefore, we also examine how the Raman lidar measurements, when used in conjunction with additional data sets, can be used to retrieve the aerosol scattering albedo, and how the resulting retrievals of single scattering albedo compare with measurements by airborne *in situ* instruments.

In this study, we first describe the Raman lidar and how it retrieved aerosol and water vapor profiles during this IOP. We describe how the algorithms used to retrieve aerosol and water vapor profiles from the CARL data were modified to reduce impacts associated with a general loss of sensitivity of the system that occurred prior to the experiment. The impacts of these modifications are discussed along with the results of comparisons of the retrieved water vapor and aerosol profiles with remote and *in situ* measurements. Next, the CARL measurements are combined with airborne Sun photometer measurements of aerosol optical thickness and *in situ* measurements of aerosol scattering and absorption to retrieve estimates of the aerosol single scattering albedo and refractive index. Finally, modifications recently implemented to CARL that have significantly enhanced the ability of this system to measure aerosol and water vapor profiles are discussed.

## **2.0 Raman Lidar**

CARL autonomously measures profiles of aerosols, clouds and water vapor in the low to mid troposphere throughout the diurnal cycle [Goldsmith *et al.*, 1998]. A tripled Nd:YAG laser, operating at 30 Hz with 300-350 millijoule pulses, is used to transmit light at 355 nm. A telescope collects the light backscattered by molecules and aerosols at the laser wavelength and the Raman scattered light from water vapor (408 nm) and nitrogen (387 nm) molecules. Profiles of water vapor mixing ratio, relative humidity, aerosol backscattering, and aerosol extinction are derived routinely using a set of automated algorithms [Turner *et al.*, 2002]. Water vapor mixing

ratio profiles are computed using the ratio of the Raman water vapor signal to the Raman nitrogen signal. Relative humidity profiles are computed using these profiles and the temperature profiles from a collocated Atmospheric Emitted Radiance Interferometer (AERI). The water vapor mixing ratio profiles are integrated with altitude to derive precipitable water vapor (PWV). Profiles of aerosol scattering ratio are derived using the Raman nitrogen signal and the signal detected at the laser wavelength. Aerosol volume backscattering cross section profiles are then computed using the aerosol scattering ratio and molecular scattering cross section profiles derived from atmospheric density data. Aerosol extinction profiles are computed from the derivative of the logarithm of the Raman nitrogen signal with respect to range. Aerosol optical thickness (AOT) is derived by integration of the aerosol extinction profile with altitude. The copolarized and cross-polarized signals (with respect to the laser beam's polarization) are also measured at the laser wavelength. These signals are used to derive the linear depolarization, which is defined as the ratio of the backscattered signals that are polarized orthogonal and parallel to the linearly polarized outgoing laser beam.

### **3.0 CARL Data Analysis**

CARL was considered a critical component of this IOP, and significant efforts were undertaken to ensure that the laser was functioning normally during the entire experiment and that no significant downtime periods occurred. Indeed, overall, CARL operated over 90% of the time during the IOP; malfunctions of the air conditioner in the CARL enclosure were responsible for most of the brief periods when the lidar did not operate. However, the degree to which the sensitivity of CARL had declined since about the end of 2001 was not fully appreciated by the participants. Examples of the impacts of this decrease can be seen in Figure 1, where the random errors associated with the retrievals of the aerosol backscatter coefficient and water vapor mixing ratio at an altitude of about 2 km, and the maximum altitudes of the water vapor mixing ratio retrievals are shown as a function of time for both daytime and nighttime operations. The maximum altitudes are defined here as the lowest altitude where the random error reaches 25%. The peak signal strength decreased by roughly a factor of 3-4 between early 2001 and May 2003. The modifications and upgrades to CARL that were

subsequently performed in 2004 to restore and significantly improve its water vapor and aerosol measurement performance are discussed in section 7.

The loss in sensitivity of CARL impacted the automated algorithms that are used to retrieve aerosol and water vapor profiles. *Turner et al. (2002)* describe these algorithms in detail. The main impacts of the decreased sensitivity include: 1) significantly higher random noise component in the retrieved profiles, 2) reduction in the maximum altitude to which the aerosol profiles can be retrieved, and 3) occasional large systematic errors in the retrieved profiles due to errors in how the automated algorithms determine the overlap corrections that need to be applied to the high channel data. The third impact arises due to the manner in which CARL was designed to periodically check, and if necessary, readjust the alignment between the outgoing laser beam and the telescope field of view. The high altitude channels, which are used for retrievals for altitudes above about 1-2 km, use a narrow (0.3 mrad) field of view in order to reduce interference from background skylight and are particularly sensitive to this alignment. These alignments checks are normally performed automatically every few hours by adjusting the alignment of the final steering mirror, which positions the outgoing laser beam in the detector's field of view to maximize the signal strength in the high nitrogen signal. However, during the aerosol IOP, the signal strengths were so low due to the loss of sensitivity that the system erroneously concluded that it was cloudy every time it attempted to perform an alignment "tweak", and as a result aborted each alignment check. Thus, no automated alignment tweaks were performed. This resulted in many periods during the IOP where the alignment apparently drifted away from optimal and consequently adversely impacted the quality of the aerosol products. Occasionally during the IOP, the system was recognized to be out of alignment and a manual alignment tweak was then performed, but this process occurred too infrequently to greatly improve the data quality.

The inability to accurately monitor, and if necessary, adjust the system alignment particularly impacted the aerosol extinction retrievals. Aerosol extinction is calculated by computing the derivative with respect to range of the logarithm of the nitrogen signal. Therefore, any instrument-induced features must be accounted for before the extinction profile can be retrieved. The main instrument feature to account for is the overlap function in the nitrogen channels. The low channel achieves full overlap (i.e., overlap function is unity) beyond approximately 800 m,

while the high channel achieves full overlap around 5 km. Therefore, one might compute the extinction profile from the low channel from 800 m to 5 km and use the high channel above 5 km. However, above approximately 1500 m, the signal-to-noise in the low channel is too low to adequately (i.e., with random errors less than 20%) retrieve aerosol extinction. Therefore, the high channel data must be used well below the region of full overlap, which implies that an overlap correction must be determined and subsequently applied to the high channel data. The automated algorithms attempt to account for the drifting overlap corrections. However, the region where the low and high channels were merged was very noisy due to the lower maximum range of the low channel data, and there were obvious problems with some periods where poor alignment is suspected.

The automated algorithms were modified in an attempt to reduce or remove these adverse impacts [Turner *et al.*, 2003a]; these modifications are summarized here. A number of changes were made to both the water vapor and aerosol retrieval algorithms. The algorithms used to compute aerosol scattering ratio and aerosol backscatter coefficient were modified in the following manner. First, the altitude range over which the low and high aerosol scattering ratios were merged was lowered from 1.5-1.9 km to 1.0-1.5 km. This significantly reduced the noise in the merge region. Second, the near-field overlap function for the aerosol scattering ratio derived from the low channel data was updated using the measurements acquired during the May 2003 Aerosol IOP. The initial processing had used an overlap correction based on data acquired during 1999 and so was out of date. This modification changed aerosol backscattering values by as much as 20% within the lowest 200 meters. Third, a new routine was developed and implemented to detect large changes in the system alignment. Manual inspection of the CARL data indicated that there were periods when the lidar's alignment obviously drifted. However, since the automated alignments did not function correctly, the previous algorithms assumed the alignment was constant. The revised algorithms were designed to search for obvious gross changes in the lidar returns and to treat the changes as alignment periods.

The algorithms that derive aerosol extinction were also modified. The vertical resolution of the low channel nitrogen data was increased by about a factor of two to improve the signal-to-noise ratio in the extinction profile. Turner *et al.* [2002] discuss how the vertical resolution varies with altitude for the derived aerosol extinction profiles. A near-field overlap correction



was computed and applied to the low nitrogen channel so that aerosol extinction could be computed directly from this channel below the altitude of full overlap, and so extend the extinction calculations from 800 m to about 400 m. The correction was determined using procedures similar to those described by *Wandinger and Ansmann* [2002]. Modifications were also made to the procedures that determine the appropriate values of the aerosol extinction/backscatter ratio ( $S_a$ ) to use in computing aerosol extinction. *Turner et al.* [2002] discuss how the aerosol extinction algorithms use the derived  $S_a$  values along with the derived aerosol backscatter coefficient to compute aerosol extinction. Consequently, when the aerosol loading is low ( $< \sim 0.05$ ), so that the relative error in the extinction derived from the Raman nitrogen channel is high ( $> \sim 30\%$ ), the extinction is derived from the product of the  $S_a$  value interpolated/extrapolated to this time and altitude and the aerosol backscatter coefficient. The modifications were made to reduce the possibility that erroneous values of  $S_a$  were used in the aerosol extinction computations.

#### **4.0 May 2003 Aerosol IOP**

The Aerosol IOP was conducted between May 5-31, 2003 over the ARM SGP CRF site (36.606 N, 97.50 W, 315 m). This experiment was designed to use ground and airborne measurements of aerosol absorption, scattering, and extinction to characterize the routine ARM aerosol measurements, and help resolve differences between measurements and models of diffuse irradiance at the surface. The assessments of aerosol optical thickness and aerosol absorption were carried out in conjunction with measurements of downwelling direct and diffuse irradiance as a function of wavelength and altitude. The IOP carried out a variety of closure experiments on aerosol optical properties and their radiative influence. Additional efforts were directed toward the measurement of cloud condensation nucleus concentration as a function of supersaturation and relating CCN concentration to aerosol composition and size distribution.

During the mission, an extensive suite of instruments were deployed on board the Center for Interdisciplinary Remotely-Piloted Aircraft Studies (CIRPAS) Twin Otter aircraft [*Bluth et al.*, 1996; *Bane et al.*, 2004]. The Twin Otter performed 16 daytime research flights over the SGP site during the IOP. The aircraft carried an Edgetech chilled mirror sensor to measure water

vapor density and instrumentation from the University of Washington to perform in-situ measurements of aerosol absorption (Particle Soot Absorption Photometer (PSAP)) and scattering (TSI nephelometer). Aerosol extinction and water vapor density were derived from measurements acquired by the NASA Ames Airborne Tracking 14-channel Sun photometer (AATS-14) [Schmid *et al.*, 2005]. Additional measurements were acquired as part of the ARM In Situ Aerosol Profiling (IAP) measurement program. In this program, measurements of water vapor and sub-micrometer aerosol scattering, backscattering, absorption and water vapor are acquired by *in situ* instruments on a small Cessna 172N aircraft flown 2-3 times per week on a long term (i.e. multi-year) basis [Andrews *et al.*, 2004]. The IAP instrument suite includes a Vaisala Humicap 50Y capacitive sensor to measure ambient relative humidity. Additional water vapor profile measurements were acquired by Vaisala RS-90 radiosondes routinely launched at this site. These airborne and radiosonde measurements were used to assess the CARL measurements of water vapor and aerosol extinction profiles.

A wide range of aerosol and water vapor conditions were observed over the ARM SGP site during the IOP. Ferrare *et al.* [2005] provide an overall description of the aerosol conditions observed during the IOP and how the conditions observed during May 2003 compare with other periods.

## **5.0 Intercomparisons**

### **5.1 Water Vapor**

Several comparisons were made to assess the CARL water vapor retrievals. The IOP water vapor comparisons include both the standard Vaisala RS-90 radiosonde water vapor profiles, as well as the radiosonde water vapor profiles that have been scaled to match the PWV measured by the ARM SGP MWR. This MWR scaling procedure has been adopted by ARM because this scaling has significantly reduced the sonde-to-sonde variability and has reduced the residuals between measurements and models of high spectral infrared radiance [Turner *et al.*, 2003b]. The uncertainty in the MWR PWV is about 3%. Similarly, CARL is also calibrated such that the total column water vapor from the Raman lidar matches the MWR PWV [Goldsmith *et al.*, 1998;

Turner and Goldsmith, 1999]. These water vapor comparisons were performed for altitudes between 0.1-3.0 km to match the nominal daytime altitude range of CARL. Enhanced background skylight limited CARL water vapor retrievals during daytime operations to altitudes below about 3 km for data acquired during the May 2003 Aerosol IOP.

Figure 2 shows examples of water vapor and aerosol extinction profiles acquired on May 22. Profiles that were derived using normal (“old”) processing are shown as well as those derived using the modified (“new”) algorithms. The new algorithms include the modifications performed to the aerosol retrieval algorithms described in the previous section. In addition, a new set of overlap corrections for deriving the low and high channel water vapor mixing ratio profiles were also determined from the CARL data. Results from previous water vapor IOPs indicated that the water vapor calibration is very stable, and that the uncertainty in the water vapor calibration is reduced when a single calibration is computed for an entire month [Turner *et al.*, 2003b; Revercomb *et al.*, 2003; Ferrare *et al.*, 2004]. Consequently, a single water vapor calibration was computed for May 2003. Updates to the CARL water vapor overlap function that are included in the modified algorithm slightly increased water vapor below about 1 km.

Water vapor profiles derived from the AATS-14 [Schmid *et al.*, 2004a] and from the Edgetech 137-C3 chilled mirror hygrometer on board the CIRPAS Twin Otter are also shown in Figure 2a. AATS-14 measures the transmission of the direct solar beam in 14 spectral channels (354 to 2139 nm). AATS-14 is an enhanced version of the AATS-6 instrument [Matsumoto *et al.*, 1987]. The methodology for data reduction, calibration, and error analysis for this instrument are described by [Russell *et al.*, 1993; Schmid and Wehrli, 1995; Schmid *et al.*, 1998, 2001, 2003, 2004a,b]. The AATS-14 channels are chosen to allow separation of aerosol, water vapor, and ozone transmission. From these slant-path transmissions are retrieved total optical thickness in 13 narrow wavelength bands and the columnar amounts of water vapor and ozone. In addition to the corrections for Rayleigh scattering and O<sub>3</sub> absorption, some channels require corrections for NO<sub>2</sub>, H<sub>2</sub>O and O<sub>2</sub>-O<sub>2</sub> absorption. Cross-sections were computed using LBLRTM 6.01 [Clough and Iacono, 1995] with the CKD 2.4.1 continuum model using the HITRAN 2000 (v 11.0) line-list [Rothman *et al.*, 2001; Rothman and Schroeder, 2002] (including an update for water vapor from April 2001, see <http://www.hitran.com/hitran/updates.html>). NO<sub>2</sub> cross-sections not included in LBLRTM 6.01 were taken from Harder *et al.* [1997]. NO<sub>2</sub> was assumed

constant at  $2 \times 10^{15}$  molecules- $\text{cm}^{-2}$ . Differences among the water vapor profiles are generally less than 10%.

CARL water vapor profiles were compared with similar profiles derived from the Vaisala RS-90 radiosondes, Vaisala RS-90 radiosondes scaled to match the MWR PWV, Edgetech 137-C3 chilled mirror, AATS-14 Sun photometer, and Vaisala 50Y Humicap capacitive sensor. The chilled mirror sensor and AATS-14 were deployed from the Twin Otter and the Vaisala Humicap sensor was deployed from the IAP Cessna aircraft. Example profile comparisons that show the CARL, AATS-14, and chilled mirror profiles are shown in Figure 3. The comparisons were made for those cases when the Twin Otter was within 30 km and 30 minutes of the CARL measurements at the SGP site. Only those cloud-free regions where all three sensors measured water vapor profiles that were coincident and collocated are shown in Figure 3.

Figure 4 shows examples of the results of the individual comparisons with the CARL water vapor profiles in terms of regression analyses. The results from the various individual regressions are shown in Table 1. Mean bias differences for water vapor comparisons between 0 and 3 km are also shown in Figure 5. Radiosondes were launched at the ARM SGP CRF site four times per day (0530, 1130, 1730, 2330 UT) so that water vapor comparisons were performed with both daytime and nighttime radiosondes. Comparisons were performed with both the nominal Vaisala RS-90 water vapor measurements, as well as the Vaisala RS-90 profiles scaled to match the MWR PWV. As expected, the CARL water vapor profiles, which are calibrated using the MWR PWV, were generally in good agreement with the MWR-scaled radiosonde measurements, as bias differences were less than about 3%. When compared with these MWR scaled radiosonde profiles, the CARL daytime water vapor profiles were slightly (~3%) drier than the nighttime profiles. Previous attempts at investigating diurnal trends in the CARL profiles had revealed much larger (>10%) diurnal biases [*Turner and Goldsmith, 1999; Linne et al., 2001*]. *Turner et al. [2000]* found that these diurnal variations could be reduced by manually characterizing the relationship between the daytime and nighttime modes. During daytime operations, a neutral density filter is inserted into the optical detector path in the narrow field of view water vapor channel to reduce background skylight. Subsequent investigations found improved ways of characterizing how the system response varies with and without this neutral density filter; the automated algorithms were then modified to incorporate this

information. These Aerosol IOP comparisons indicate that the diurnal CARL bias has indeed been substantially reduced.

The results in Table 1 also show that, when comparing MWR scaled and unscaled radiosonde profiles, the impacts of MWR scaling are larger during the day (~7%) than at night (~2%). This indicates that there is a daytime dry bias of the Vaisala RS-90 sensor. Previous comparisons of PWV from RS-90 sondes and MWRs at the ARM SGP and TWP sites have found that the radiosonde PW is consistently 6-8% drier for daytime soundings than for nighttime soundings [Miloshevich, 2004, personal communication]. Other comparisons have also found a daytime dry bias of about 3-4% in the RS-90 sondes [Vance *et al.*, 2004] and that this bias is due to solar heating of the air stream inside these sondes [Nash *et al.*, 2003].

Mean bias differences shown in Figure 5 indicate that the CARL and MWR-scaled radiosonde measurements tended to be 5-10% wetter than the chilled mirror sensor, RS90 radiosondes, and Sun photometer. The largest differences were generally found for low relative humidity conditions. The reasons for such large differences are not presently clear, but may be related to the use of the MWR PWV as a calibration standard since both the CARL and scaled radiosonde water vapor profiles are calibrated to match the MWR PWV. Previous nighttime comparisons of PWV derived by scaling the Raman lidar water profiles to match a chilled mirror sensor on the SGP tower with the MWR PWV values showed that the two techniques had the same responses to water vapor (i.e. slope near unity), but that there was an offset of 0.95 mm (3-4%) with the MWR PWV higher by this amount than the tower-scaled Raman lidar PWV values [Revercomb *et al.*, 2003]. Previous comparisons have also found better agreement between the CARL and Vaisala 50Y capacitive sensor measurements on the IAP Cessna aircraft [Ferrare *et al.*, 2002]. The large differences shown in Figure 5 are most pronounced at low relative humidity conditions. The Vaisala 50Y water vapor profiles were consistently lower than the chilled mirror profiles on the four flights when the IAP Cessna and Twin Otter aircraft flew in close formation.

In order to further examine these water vapor measurements, we examined the behavior of the water vapor profiles near the base of a low water cloud. Assuming a relative humidity of 100% at cloud base, Whiteman *et al.* (2001) used Raman lidar returns near cloud base to examine the water vapor calibration characteristics of a similar Raman lidar system. Figure 6 shows the

water vapor and relative humidity profiles near cloud base on May 17. The Vaisala radiosonde was launched at 17:55 UT, the CARL profile represents an average between 18:00 and 19:00 UT, and the Twin Otter within cloud measurements occurred between 19:05-19:10 UT. Throughout May 17, and into May 18, a uniform stratus cloud was located over the SGP site. Lidar and *in situ* cloud particle and liquid water measurements on the Twin Otter indicated that cloud base was at about 0.95 km and cloud top was near 1.5 km. The water vapor and RH profiles shown in Figure 6 also show similar systematic differences, with the CARL and MWR scaled Vaisala radiosonde profiles 5-10% higher than the Vaisala RS90 and Twin Otter chilled mirror profiles. Above cloud base and within the cloud, the MWR-scaled Vaisala profile shows an unrealistically high RH value of 105%, which strongly suggests that, at least in this particular case, the MWR scaling produced a high bias of about 5%. Cloud attenuation rapidly decreased the signal/noise ratio so that CARL water vapor profile was unreliable above cloud base. The RS90 profile is closer to the expected 100% value within the cloud, but is slightly low by a few percent. The chilled mirror and RS90 water vapor profiles are in very good agreement. The difference between the chilled mirror and RS90 RH profiles is because the temperature profile recorded on the Twin Otter was about 0.5 K higher than the radiosonde temperature profile. At these ambient conditions, a 0.5 K temperature difference will result in a difference of about 3% in RH, so that chilled mirror and RS90 RH profiles are in agreement when accounting for the temperature difference. Consequently, this case suggests that the MWR scaling is about 5% high, and the *in situ* measurements are a few percent low. Subsequent to these analyses, an independent assessment of the MWR retrieval algorithms found that the MWR precipitable water vapor (PWV) computed since April 2002 is 3% too high due to the use of an older [Rosenkranz, 1998] 22.2 GHz line width instead of updated HITRAN [Rothman *et al.*, 2001, Rothman and Schroeder, 2002] line width. Liljegren *et al.* [2004] discuss the impact of the 22 GHz linewidth. Accounting for the improved linewidth will lower the MWR-scaled sondes and CARL observations by 3%, and will bring these measurements into closer agreement with the other water vapor measurements. A new Value-Added Procedure (VAP) that uses the most current absorption models as well as improved retrieval techniques is currently being implemented to provide revised MWR PWV retrievals [Turner *et al.*, 2004].

## 5.2 Aerosol

The aerosol extinction profiles derived from the CARL measurements were also compared with extinction profiles derived from the airborne remote sensing and *in situ* instruments on the Twin Otter and the *in situ* instruments on the IAP Cessna aircraft. The AATS-14 profiles were derived in the manner as described by *Schmid et al.* [1998, 2001, 2003, 2004a,b]. AATS-14 was calibrated at Mauna Loa Observatory, Hawaii, just before and after the IOP. The spectral aerosol extinction profiles, like the water vapor profiles, were derived by first smoothing and then differentiating the optical thickness profiles. Note that the Sun photometer optical thickness profiles may occasionally increase (decrease) as the plane ascended (descended) such that the aerosol extinction may become negative. This can happen because the path between the Sun photometer and the Sun passes through a horizontally inhomogeneous, time-varying atmosphere. AATS14 measurements have been used in several experiments to assess *in situ* and remote sensing (e.g. lidar) profiles of aerosol extinction [*Schmid et al.*, 2000; 2003a,b; 2005].

Aerosol extinction profiles were also derived from the light scattering and absorption measurements on the Twin Otter and IAP Cessna. On the Twin Otter, light scattering was measured using a TSI 3563 three wavelength nephelometer (450, 550, 700 nm). This nephelometer was calibrated against particle-free air and CO<sub>2</sub> prior to the field deployment and zeroed with particle-free air before each flight. Nephelometer total scatter is corrected for angular nonidealities according to *Anderson and Ogren* [1998]. Scattering is corrected to ambient temperature, pressure, and RH at the Twin Otter aircraft location. The correction to ambient relative humidity was made using measurements of the aerosol humidification factor and relative humidity that were also acquired on the Twin Otter. The relative humidity used for these corrections was derived using dew point temperatures measured by the Edgetech chilled mirror hygrometer. The hygroscopic behavior of the aerosol was determined from the three Radiance Research nephelometers operating at different RH values. The dependence of light-scattering on RH,  $f(\text{RH})$ , was parameterized based on the work of *Kasten* [1969; see also *Gasso et al.*, 2000].

Aerosol light absorption was measured using a three wavelength (467, 530, and 660 nm) Particle Soot Absorption Photometer (PSAP) made by Radiance Research (Seattle, WA). The

absorption data were corrected using the procedures described by *Bond et al.* [1999]. Because the absorption was measured just downstream of the TSI nephelometer, it was measured under sub-ambient RH (a nominal 30% below ambient). However, following *Hegg et al.* [1997], no correction was made for the higher RH of the ambient air since experimental data for such a correction are lacking. A study modeling sulfates with black carbon cores by *Redemann et al.* [2001] suggests that absorption humidification factors are negligible for a wide range of atmospheric conditions.

The scattering signals were reported at 8-sec intervals, which roughly represents the sampling interval of the nephelometers as determined by instrument volume, flow rate and instrumental (electronic) averaging times. This coincides with 20-meter intervals during a 500 feet/minute spiral ascent. Unrealistic data points due to instrument malfunction, adjustment in flight and data acquisition problems have been removed from all data sets. The PSAP data have been smoothed with a 64-second boxcar average to remove mean-zero spikes caused by rapid changes in humidity.

Aerosol extinction profiles were also derived in a similar manner from the nephelometer and PSAP measurements acquired on the IAP Cessna aircraft. During the May 2003 IOP, this was a single wavelength instrument with absorption reported at 550 nm. *Andrews et al.* [2004] give a complete description of these procedures which are summarized here. In order to compare these *in situ* measurements with the remote sensing measurements, these measurements were also adjusted to ambient conditions. Here the scattering coefficients were adjusted to ambient RH in a similar manner as was done for the Twin Otter measurements; however, in this case, the humidification factor was derived using the RH-dependent scattering measured at the surface and assuming this factor is constant with altitude [*Sheridan et al.*, 2002; *Andrews et al.*, 2004]. Although there can be significant vertical variations in this factor due to variability in the aerosol composition and/or deliquescence properties, computations of AOT using this assumption found that using large variations in the humidification factor resulted in small (<15%) differences in the total AOT [*Andrews et al.*, 2004]. The absorption data were not corrected for possible hygroscopic growth. To account for the presence of coarse (aerodynamic diameter > 1  $\mu\text{m}$ ) particles, which are not sampled by the IAP instruments, a correction was made on the basis of measurements of supermicrometer particles made at the surface. The ratio of submicrometer to



supermicrometer scattering measured at the surface was assumed to hold for all altitudes measured in the IAP flights. This assumption probably results in an upper limit of the amount of coarse aerosol present and thus probably overestimates aerosol extinction.

Figure 2b shows an example of the aerosol extinction retrievals for May 22. Profiles derived from the CARL data using both the old and revised algorithms are shown along with the profile derived from the AATS-14 data. Note how the revised algorithm has significantly reduced the aerosol extinction in the lowest kilometer and reduced the oscillations in the profile between 1 and 2 km. The CARL and AATS-14 profiles are generally in good agreement near the top of the boundary layer, but the CARL profile is slightly higher above this layer. Figure 7 shows the comparisons of aerosol extinction profiles derived from the CARL and AATS-14 data, and from the *in situ* scattering and absorption measurements on board the Twin Otter. As in the case of water vapor, these profiles represent cases when the Twin Otter measurements were within 30 minutes and 30 km of the SGP site; the majority of the cases, the measurements were coincident and within 10 km of the ARM SGP site. The CARL aerosol extinction measurements at 355 nm were converted to 450 nm in order to directly compare with the *in situ* measurements shown in Figure 7. In those cases when AATS-14 measurements were available, the CARL profiles were converted from 355 nm to 450 nm using the aerosol Ångström exponent derived from the AATS-14 extinction measurements (at 354 and 450 nm) at each altitude. In those cases when AATS-14 measurements were not available, the conversion was made using the Ångström exponent derived from the *in situ* scattering and absorption measurements (450-700 nm). The CARL profiles can be seen to generally match the shapes of the profiles measured derived from the AATS-14 and *in situ* measurements, although on some days the CARL profiles are somewhat higher than the other profiles. The error bars on the measurements represent the variability of the measurements over the period that the profiles were derived; this period generally varied between 10 and 60 minutes. Note that the CARL and AATS-14 profiles are in general agreement within this measurement variability.

Figure 8 shows, in the form of regressions, how the CARL aerosol extinction measurements compare with the AATS and *in situ* retrievals of aerosol extinction. The AATS-14 comparison is at 355 nm and the *in situ* aerosol extinction is at 450 nm. Table 2 also shows the results of these regressions. Bias differences were generally about 0.025-0.033 km<sup>-1</sup>. The aforementioned

reduction in CARL sensitivity led to increased calibration errors, larger random errors, and greater uncertainties in maintaining proper alignment, all of which contributed to these large differences. The extensive modifications made to the CARL automated algorithms reduced but could not eliminate these adverse effects. Note that, as shown in Figure 9, the largest relative differences were found for low ( $<0.05 \text{ km}^{-1}$ ) aerosol extinction values and that the differences were significantly less ( $\sim 10\%$ ) for higher ( $0.15\text{-}0.3 \text{ km}^{-1}$ ) values of aerosol extinction. *Masonis et al.* [2002] showed that the uncertainty in the Institut für Troposphärenforschung (IfT) nighttime Raman lidar measurements was about 30% and higher for aerosol extinction levels below about  $0.03 \text{ km}^{-1}$  and decreased to about 10% for aerosol extinction level higher than about  $0.15 \text{ km}^{-1}$ ; these levels are comparable to the bias differences noted here for CARL daytime measurements. The reason(s) for the high bias, especially for low aerosol extinction values, is(are) not clear, but may be related in part to the temperature dependence of Raman scattering. For Raman lidars such as CARL that use very narrow bandwidth filters to reduce background skylight, the change in the Raman scattering with temperature should be considered [*Whiteman et al.*, 2003a,b]. For a narrow bandpass filter, the integrated intensity of the Raman scattering feature across the scattering band will be temperature sensitive. *Whiteman et al.* [2003b] indicated that neglecting these impacts may introduce significant ( $>10\%$ ) biases in the Raman lidar aerosol retrievals for aerosol scattering ratios greater than about 1.2; more recent modeling has indicated that such biases are possible but are more likely restricted to lower aerosol scattering ratios ( $\sim 1.08$ ) [*Whiteman*, 2004, personal communication].

A previous comparison of Raman lidar aerosol extinction measurements with aerosol extinction derived from *in situ* measurements found that the lidar values were about 30% higher than the *in situ* measurements [*Masonis et al.* 2002]. Potential reasons for these differences include supermicrometer particle losses in the aircraft inlet, underestimation of the humidification factor used to adjust the *in situ* measurements to ambient humidity, underestimation of the relative humidity, and temporal and spatial variability. *Schmid et al.* [2004] investigated column closure for aerosol extinction during the IOP and found that the aerosol extinction measurements from the *in situ* scattering and absorption measurements was about 10-20% lower than derived from the Sun photometer measurements. The observation that remote sensing retrievals of aerosol extinction and/or AOT is often higher than corresponding *in*

*situ* retrievals has been reported in several previous studies [e.g. *Ferrare et al.*, 2000a,b; *Hartley et al.*, 2000, *Schmid et al.*, 2000, *Kato et al.*, 2000, *Andrews et al.*, 2004]. Although these studies have suggested several potential mechanisms that can produce these differences, including the possible causes listed above, the specific reason(s) for these differences have not been definitively identified.

## 6.0 Aerosol Retrievals

One of the main objectives of the May 2003 Aerosol IOP was to measure aerosol optical properties (scattering, absorption, and extinction) using a number of different instruments simultaneously with measurements of direct and diffuse solar radiation in order to better understand and model the impact of aerosols on direct and diffuse radiation. Particular emphasis was placed on accurately characterizing measurements and retrievals of aerosol absorption and aerosol single scattering albedo. Consequently, we also attempted to retrieve estimates of the aerosol single scattering albedo and the effective complex refractive index using a combination of active (lidar) and passive (Sun photometer) measurements along with *in situ* measurements of the aerosol size distribution. For these retrievals, we used methods similar to those used by *Ferrare et al.* [1998] and *Redemann et al.* [2000], who used a combination of lidar and *in situ* measurements to derive estimates of the aerosol complex refractive index and single scattering albedo.

The aerosol size distributions measured by a PMS Passive Cavity Airborne Spectrometer Probe (PCASP), which measured the number of particles in twenty size bins covering particle diameters between 0.1 and 3  $\mu\text{m}$ , were used in a series of Mie computations to compute the aerosol extinction/backscattering ratio ( $S_a$ ) and aerosol extinction coefficient. Since the PCASP measured “dry” aerosol sizes, the aerosol size distributions were adjusted to ambient relative humidity conditions by comparing the PCASP size distributions with the ambient size distributions measured by a Droplet Measurement Technologies (DMT) Cloud, Aerosol and Precipitation Spectrometer (CAPS) system [*Baumgardner et al.*, 2002]. In this process, the adjustment was derived by determining the appropriate multiplicative correction to apply to the PCASP size distribution in order to make the PCASP and CAPS size distributions match in the

region of overlap (particle diameter between about 0.8 and 2.7  $\mu\text{m}$ ); this same adjustment was then applied to all particle sizes measured by the PCASP. The particle growth factors computed in this manner were consistent with those derived from ground-based TDMA measurements [Gasparini *et al.*, 2005]. The lidar measurements of  $S_a$  (355 nm) and the Ångström exponents ( $\text{\AA}$ ) that were computed using the aerosol extinction profiles at 450 nm and 675 nm retrieved from the AATS-14 airborne measurements were used to constrain the retrievals of refractive index and aerosol single scattering albedo. Because of the larger uncertainties that were associated with CARL retrievals acquired during low aerosol extinction conditions, only those cases when the aerosol extinction coefficients were greater than  $0.1 \text{ km}^{-1}$  were considered. In addition, the high biases in the CARL measurements would likely affect both aerosol backscattering and extinction, in which case the ratio of aerosol extinction to backscatter ( $S_a$ ) would have smaller relative biases than either backscatter or extinction.

An example of these results for data acquired during May 25 is shown in Figure 10. The aerosol extinction profiles derived from CARL, airborne *in situ* (nephelometer scattering+PSAP absorption), and AATS-14 measurements are shown along with measured and derived aerosol optical properties (450 nm). The results for this case and the other cases are listed in Table 3. The refractive indices listed represent values at ambient humidity. For the profile shown in Figure 10, satellite imagery and back trajectory analyses indicate that the elevated aerosol layers located between about 2.6 and 3.6 km were smoke layers produced by Siberian forest fires [Damoah *et al.*, 2004; Jaffe *et al.*, 2004]. CARL and the airborne remote and *in situ* sensors observed these thin layers between May 25-28. The trajectory and aerosol transport models indicate that the smoke was lofted into the upper troposphere (200-400 hPa) and was transported over much of the Northern U.S. and Canada during May and June 2003. The CARL and airborne *in situ* measurements of very low relative humidity (<5%) associated with these layers is consistent with the descent of these layers from the upper troposphere. The relatively large particle sizes for the smoke layers shown in Figure 10 are consistent with other observations of long range transport of aged smoke [Muryama *et al.*, 2004; Mattis *et al.*, 2004]. The values of aerosol single scattering albedo ( $\omega_0$ ) derived from *in situ* measurements of aerosol scattering and absorption and retrieved using the method described above are in good agreement for both the smoke and the boundary layer aerosols and indicate that both types of aerosols were relatively

non-absorbing. Similar values of  $\omega_0$  for this smoke were also found using multiwavelength lidar retrievals for lidar data acquired over Tokyo, Japan and Leipzig, Germany [Muryama *et al.*, 2004; Mattis *et al.*, 2004]. The derived real refractive indices ( $m_r$ ) are also consistent with those derived for long range transport of smoke over Europe observed during 1998 [Wandinger *et al.*, 2002]. Retrievals performed for other days during the May 2003 Aerosol IOP found that  $\omega_0$  varied between 0.91-0.98;  $m_r$  varied between 1.48-1.60 and  $m_i$  varied between 0.002 to 0.007. The results shown in Table 3 indicate that the retrieved values are generally in good agreement with the values derived from the *in situ* measurements of scattering and absorption on the Twin Otter.

## 7.0 CARL Modifications/Upgrades

After the Aerosol IOP, several efforts have been undertaken to characterize and modify the Raman lidar to restore and/or improve its sensitivity. These efforts, which are summarized here, have included modifications to the optical components as well as the data recording electronics. The initial modifications included relatively simple changes to the system in the hope that more extensive changes would not be necessary. First, the external window through which the telescope views the laser light scattered by the atmosphere, and the lens on the telescope which expands the outgoing laser beam and consequently decreases the divergence of the laser beam were both replaced. Mirrors which direct the laser beam within the optical path were also replaced. The alignment of all the components of the optical train was checked and adjusted to give maximum throughput. The impact of these changes was to slightly (~20%) increase the signal levels in the elastic (i.e. Rayleigh+Mie) scattering channels, but not enough to restore desirable performance levels.

Close examination of the primary and secondary mirrors in late 2003 revealed that the reflective surfaces on these mirrors had degraded. Consequently, these mirrors were removed and refurbished. In addition, the narrow bandwidth interference filters that are used to select the appropriate wavelengths for the return signals and reject the background skylight were also replaced. The new interference filters increased the transmission throughput from about 40% to about 60%. The result of these changes was to restore signal strengths to levels comparable to,

or slightly higher, than those obtained in early 1998 when the system had begun routine operations in earnest. In addition, the motor-driven mirror mount that was used to periodically check the alignment of the system was replaced. Unlike the previous motor mount, the new mount has the ability to return the alignment to the exact alignment position in the event of an interruption in the alignment process.

Next, the photon counting electronics were replaced with units from Licel GbR that combine both photon counting and analog-to-digital (A/D) conversion. Similar electronics have been successfully demonstrated in the NASA GSFC Scanning Raman lidar system [Whiteman *et al.*, 2004; 2005]. Previously, only photon counting electronics were used in order to maximize the detection capabilities for the weak Raman water vapor signals and to have a similar detection and electronics for all channels in the system. Although photon counting is optimal for detecting weak water vapor signals, the strong return signals from the elastic and nitrogen Raman channels, especially close to the lidar, required the use of neutral density filters in order to prevent pulse pile-up in the photon counting detection electronics.. Therefore, much of the return signals in the elastic scattering and Raman nitrogen channels were simply discarded in order to prevent saturation of the photomultipliers. Although this design was sub-optimal for measuring aerosol profiles, it was quite suitable and efficient for the autonomous, automated acquisition of water vapor profiles, which was the primary reason that ARM developed this system. The A/D conversion capabilities of the Licel electronics permit the detection of much stronger signals than could be obtained with the photon counting electronics alone, so that the attenuating neutral density filters could be reduced in the case of the high and low elastic (i.e. aerosol) channels, and eliminated in the case of the nitrogen Raman channels. As a result, the signal strengths in the aerosol and Raman nitrogen channels increased by a factor of about 10-20. The use of the Licel electronics also increased the maximum vertical resolution from 30 m to 7.5 m.

These modifications have resulted in a dramatic improvement in the aerosol and water vapor measurement performance of the CARL system. This increase can be seen in the large reduction in the random errors in the aerosol backscattering and water vapor computations in mid-2004 shown in Figure 1. The maximum altitude for which water vapor profiles could be derived also significantly increased at this time. Examples showing the impacts of these improvements on the

retrievals of water vapor mixing ratio and aerosol scattering ratio can also be seen in Figure 11. Water vapor mixing ratio, aerosol scattering ratio, and the associated random errors are shown for two days: September 28, 1998 and September 26, 2004. These results were produced using the same vertical resolutions for both cases. The PWV and AOT for these two days were similar. The first day shows performance typical for the period shortly after the lidar began routine operations, and the second day was after the system had resumed operations after the modifications described above were implemented. Nighttime measurements occur before about 12:30 UT and daytime measurements occur after this time. Note how the random errors in the water vapor and aerosol scattering ratio profiles were significantly smaller for both the daytime and nighttime measurements after the modifications were implemented.

The impacts on the aerosol extinction retrievals could not be immediately assessed because the changes to detection electronics require extensive changes to the software used to record and process these data. Work is currently underway within ARM to develop and implement the necessary changes; we expect revised data collection software to be implemented during the first part of 2005.

There are a number of reasons why these modifications are expected to improve the aerosol extinction retrievals and consequently may bring these profiles into more consistent agreement with other aerosol extinction retrievals. The increased signal strength in the nitrogen channel does permit the system to correctly and automatically monitor the alignment of the outgoing laser beam within the field of view of the telescope, and the periodic realignments are much more precise than previously. As discussed in section 3, during the IOP signal strengths were too low to allow this automatic alignment monitoring and adjustment process. There were some occasions during the IOP when the scientists and instrument operators could readily determine that the system was not properly aligned; in these cases, the system was manually realigned. However, it is likely there were other periods when the system was slightly misaligned and the impacts were not readily apparent, so that the no correction measures were taken. These adverse impacts would produce periods when the aerosol extinction was systematically either too high or too low. When the system can automatically monitor and maintain proper alignment, as was done between 1998 and 2002, the likelihood that the system is misaligned for any extended period of time (i.e. less than a few hours) is greatly reduced.

The increased signal strengths would help in other ways. As described by *Turner et al.* [2002], the CARL measurements of aerosol scattering ratio are used to derive aerosol backscattering profiles which are then used along with the CARL measurements of aerosol extinction to derive  $S_a$ . CARL aerosol extinction profiles are then derived by multiplying the aerosol backscattering profiles by  $S_a$ . Thus, the uncertainty in the derived aerosol extinction profile is determined by uncertainties in the aerosol backscattering profiles as well as uncertainties in  $S_a$ . Computing aerosol extinction from Raman nitrogen signals is difficult when the aerosol loading is low (e.g., for regions where the extinction coefficient is less than about  $0.03 \text{ km}^{-1}$ ). Therefore, the algorithms compute  $S_a$  only for those locations and periods when the aerosol extinction values are above  $0.03 \text{ km}^{-1}$  and the random error in these measurements is less than a threshold (typically 50%). The algorithms filter these  $S_a$  values, interpolate/extrapolate the values to cover all times and altitudes, and then use these filtered  $S_a$  values along with the aerosol backscatter coefficient profiles to compute aerosol extinction profiles. When the signal strength is low, random errors can often exceed the aerosol extinction random error threshold resulting in a very sparse set of  $S_a$  measurements in time and space, which leads to larger uncertainties in the filtered set of  $S_a$  values. Increased uncertainties in the  $S_a$  values would, in turn, lead to larger uncertainties in the derived aerosol extinction profiles. Larger signal strengths will reduce the uncertainties in the derived extinction profiles by reducing the uncertainties associated with both the filtered  $S_a$  dataset and in the aerosol backscattering profiles.

## **8.0 Summary and Conclusions**

Aerosol and water vapor profiles measured by the DOE ARM SGP CRF Raman lidar (CARL) during the May 2003 Aerosol IOP were compared with aerosol and water vapor profiles measured by airborne remote sensing and *in situ* instruments. This mission represented the first extensive experiment conducted during the daytime to examine both the aerosol and water vapor measurement capabilities of this lidar. Although the lidar system operated over 90% of the time during the IOP, subsequent analyses revealed that the sensitivity of the lidar system had gradually decreased by a factor of 2-4 since late 2001 so that lidar performance during the IOP



was less than optimal. The degradation had been so gradual that the reduction had not been noticed prior to the IOP. The loss of sensitivity adversely impacted the aerosol and water vapor retrievals in several ways including: 1) significantly higher random noise component in the retrieved profiles, 2) reduction in the maximum altitude to which the aerosol profiles can be retrieved, and 3) occasional large systematic errors in the retrieved profiles due to errors in how the automated algorithms determine the overlap corrections that need to be applied to the high (i.e. narrow field of view) channel data. The results from this study highlight the need to frequently and closely monitor the performance of such lidar systems in order to insure the long term integrity of the data.

The automated routines that have been used to process the CARL aerosol and water vapor profiles since 1998 were modified in an attempt to reduce and/or remove these impacts. The modifications to the aerosol retrievals: 1) lowered the low/high channel merge region, 2) increased the vertical smoothing of low N2 channel, 3) updated the overlap correction functions, 4) developed new procedures for detecting gross alignment changes, and 5) improved the logic associated with the retrieval and use of the aerosol extinction/backscatter ratio. Modifications to the water vapor retrievals updated the overlap correction functions and changed the calibration procedure to use a single water vapor calibration constant for the entire IOP.

Water vapor comparisons were performed for altitudes between 0.1-3.0 km to match the nominal daytime altitude range of the Raman lidar water vapor measurements. The CARL profiles were generally in good (<5% bias difference) agreement with the Microwave Radiometer (MWR) scaled radiosonde measurements but were 5-10% wetter than the profiles from the unscaled radiosondes, an airborne chilled mirror sensor, and an airborne Sun photometer. The largest differences were generally found for low relative humidity conditions. The reasons for such large differences are not presently clear, but may be related to the use of the MWR PWV as a calibration standard since both the Raman lidar and scaled radiosonde water vapor profiles are calibrated to match the MWR PWV. Previous nighttime comparisons found that scaling Raman lidar water profiles to match a chilled mirror sensor on the SGP tower produced profiles that were 3-4% drier than the profiles scaled to match the MWR PWV [Revercomb *et al.*, 2003]. Subsequent analyses that indicated that the MWR precipitable water vapor (PWV) computed since April 2002 is 3% too high due to use of older [Rosenkranz, 1998]

22.2 GHz line width instead of updated HITRAN line width. MWR PWV algorithms are being modified to incorporate the updated linewidths and produce updated PWV values. The water vapor comparisons also show that the Vaisala RS90 profiles have a daytime dry bias of about 5%, which is consistent with other results [Vance *et al.*, 2004].

The Raman lidar aerosol extinction profiles were also compared with aerosol extinction profiles derived from measurements of AOT from an airborne Sun photometer and *in situ* measurements of aerosol scattering and absorption. Although the Raman lidar aerosol extinction profiles were, on average, significantly (~50%) higher than the other measurements, the largest differences were found for low ( $<0.05 \text{ km}^{-1}$ ) aerosol extinction values. Differences were significantly less (~10%) for higher ( $0.15\text{-}0.3 \text{ km}^{-1}$ ) values of aerosol extinction. Note that the absolute differences between the lidar measurements of aerosol extinction and the other retrievals is about the same as found from previous comparisons between lidar and *in situ* measurements. The aforementioned reduction in the Raman lidar sensitivity led to increased calibration errors, larger random errors, and greater uncertainties in maintaining proper alignment, all of which contributed to these differences. In addition, no attempt was made to account for the temperature dependence of Raman scattering and the potential impact on the derived aerosol backscattering and extinction profiles [Whiteman *et al.*, 2003]; modeling studies suggest that these impacts may introduce biases in the Raman lidar aerosol retrievals.

After the Aerosol IOP, several efforts have been undertaken to restore and/or improve the sensitivity of CARL. These efforts have included modifications to the detection and transmission optics, as well as using new detection electronics to include both analog-to-digital conversion as well as photon counting. The hardware modifications have been completed during 2004; data collection and processing software is currently being modified to accommodate the changes to the data streams produced by these modifications. Although the impacts of these modifications have not been fully assessed, initial results have indicated dramatic improvements in the retrievals of aerosols and water vapor for both daytime and nighttime measurements. For example, preliminary indications show that retrievals from the modified CARL system should reduce random errors in the aerosol and water vapor retrievals by an order of magnitude over those encountered during the IOP.

Since the water vapor and aerosol profiles produced by CARL are important for meeting the ARM goals discussed in section 1, for assessing the ability of aerosol transport models (e.g. Aerosol Model Intercomparison Study <http://nansen.ipsl.jussieu.fr/AEROCOM/DATA/lidar.html>) to represent the vertical distribution of aerosols, and for potential use in validating satellite measurements (e.g. AURA, CALIPSO), it would be highly desirable to more fully assess the aerosol measurement capabilities of the upgraded CARL system. In particular, comparisons of aerosol extinction profiles derived from airborne remote sensing (i.e. Sun photometry) and *in situ* instruments such as those deployed during the Aerosol IOP would be valuable for characterizing the performance of this autonomous lidar system.

### **Acknowledgements**

We wish to thank Chris Martin and the staff at the SGP site for the maintenance of CARL and for their help in the upgrade and refurbishment of this system. SGP CRF Raman lidar data were obtained from the Atmospheric Radiation Measurement (ARM) Program sponsored by the U.S. Department of Energy, Office of Energy Research, Office of Health and Environmental Research, Environmental Sciences Division. This research and the May 2003 Aerosol IOP were supported by the Office of Biological and Environmental Research of the U.S. Department of Energy as part of the ARM Program. Support for Richard Ferrare was also provided by NASA Earth Science Enterprise (now Science Mission Directorate).

## References

- Anderson, T. L., and J. A. Ogren, Determining aerosol radiative properties using the TSI 3563 integrating nephelometer, *Aerosol Sci. Technol.*, 29, 57- 69, 1998.
- Andrews E., P. J. Sheridan, J. A. Ogren, and R. Ferrare, In Situ Aerosol Profiles over the Southern Great Plains CART site, Part I: Aerosol Optical Properties, *J. Geophys. Res.*, 109, D06208, doi:10.1029/2003JD004025, 2004.
- Bane, J. M., Bluth, R., Flagg, C., Jonsson, H., Melville, W. K., Prince, M., Riemer, D. UNOLS now Oversees Research Aircraft Facilities for Ocean Science. *Eos Trans. AGU*, 85(41), 402, 2004.
- Baumgardner, D., H. Jonsson, W. Dawson, D. O'Connor and R. Newton, The cloud, aerosol and precipitation spectrometer (CAPS): A new instrument for cloud investigations, *Atmos. Res.*, 59-60, 251-264, 2002.
- Bluth, R. T, Durkee, P. A., Seinfeld, J. H., Flagan, R. C., Russell, L. M., Crowley, P. A. and Finn, P. Center for Interdisciplinary Remotely-Piloted Aircraft Studies (CIRPAS). *Bull. Amer. Meteor. Soc.* 77, 2691-2699, 1996.
- Bond, T. C., T. L. Anderson, and D. Campbell, Calibration and Intercomparison of Filter-Based Measurements of Visible Light Absorption by Aerosols, *Aerosol Sci. Technol.*, 30, 582- 600, 1999.
- Charlock, T.P., and T. Alberta, 1996: The CERES/ARM/GEWEX Experiment (CAGEX) for the Retrieval of Radiative Fluxes with Satellite Data, *Bull. Amer. Meteor. Soc.*, 77, 2673-2683.

- Clough S. A., and M. J. Iacono, "Line-by-line calculations of atmospheric fluxes and cooling rates II: Application to carbon dioxide, ozone, methane, nitrous oxide, and the halocarbons," *J. Geophys. Res.*, 100, 16,519-16,535, 1995.
- Damoah, R., N. Spichtinger, C. Forster, P. James, I. Mattis, U. Wandinger, S. Beirle, T. Wagner, and A. Stohl, Around the world in 17 days – hemispheric-scale transport of forest fire smoke from Russia in May 2003. *Atmospheric Chemistry and Physics*, Vol. 4, pp 1311-1321, 23-8-2004.
- Feingold, G., W. R. Cotton, S. M. Kreidenweis, and J. T. Davis, Impact of giant cloud condensation nuclei on drizzle formation in marine stratocumulus: Implications for cloud radiative properties. *J. Atmos. Sci.*, 56, 4100-4117, 1999.
- Ferrare, R.A., S.H. Melfi, D.N. Whiteman, K.D. Evans, M. Poellot, and Y.J. Kaufman, Raman Lidar Measurements of Aerosol Extinction and Backscattering - Part 2: Derivation of Aerosol Real Refractive Index, Single Scattering Albedo, and Humidification Factor using Raman Lidar and Aircraft Size Distribution Measurements, *J. Geophys. Res.*, 103, No. D16, 19673-19689, 1998.
- Ferrare, R.A., S. Ismail, E. Browell, V. Brackett, M. Clayton, S. Kooi, S.H. Melfi, D. Whiteman, G. Schwemmer, K. Evans, P. Russell, J. Livingston, B. Schmid, B. Holben, L. Remer, A. Smirnov, and P.V. Hobbs, Comparison of aerosol optical properties and water vapor among ground and airborne lidars and sun photometers during TARFOX, *J. Geophys., Res.*, 105, No. D8, 9917-9933, 2000a.
- Ferrare, R.A., S. Ismail, E. Browell, V. Brackett, M. Clayton, P. V. Hobbs, S. Hartley, J.P. Veefkind, P. Russell, J. Livingston, and D. Tanré, Comparisons of LASE, aircraft, and satellite measurements of aerosol optical properties and water vapor during TARFOX, *J. Geophys. Res.*, 105, No. D8, 9935-9947, 2000b.

- Ferrare, R. A., D. D. Turner, L. A. Heilman, W. Feltz, O. Dubovik, and T. Tooman: Raman Lidar Measurements of the Aerosol Extinction-to-Backscatter Ratio Over the Southern Great Plains, *J. Geophys. Res.*, 106, 20333-20347, 2001.
- Ferrare, R.A, Turner D.D., Clayton M.B., Brasseur L.H., Tooman, T.P., Goldsmith, J.E.M, Ogren, J.E., Andrews E., Raman Lidar Profiling of Aerosols and Water Vapor Over the Southern Great Plains, *ARM Program Science Team Meeting*, April 8 - 12, 2002, St. Petersburg, Florida, 2002.
- Ferrare R.A., Turner, D.D., Clayton, M., Brackett, V., Tooman,T.T., Goldsmith, J.E.M., Ogren, J.A., Andrews,E., Welton, E.J., Campbell,J.R., and Chin, M., Vertical Variability of Aerosols and Water Vapor over the Southern Great Plains, DOE ARM Science Team Meeting, Broomfield, CO, 2003, [http://www.arm.gov/docs/documents/technical/conf\\_0304/ferrare-ra.pdf](http://www.arm.gov/docs/documents/technical/conf_0304/ferrare-ra.pdf)
- Ferrare, R. A., E.V. Browell, S. Ismail, S. Kooi, L.H. Brasseur, V.G. Brackett, M. Clayton, J. Barrick, H. Linn,, A. Lammert, G. Diskin, J. Goldsmith, B. Lesht, J. Podolske, G. Sachse, F.J. Schmidlin, D. Turner, D. Whiteman, D. Tobin, H. Revercomb, B. Demoz, and P. Di Girolamo, Characterization of upper troposphere water vapor measurements during AFWEX using LASE, *J. Atmos. Oceanic Tech.*, in press, 2004.
- Ferrare, R.A., et al., The DOE ARM May 2003 Aerosol Intensive Operations Period: An Overview, manuscript in preparation, 2005.
- Gasparini, R., R. Li, D. R. Collins, R. A. Ferrare, and V. G. Brackett, Application of aerosol hygroscopicity measured at the ARM Southern Great Plains site to examine composition and evolution, submitted to *J. Geophys. Res.*, 2004.
- Gasso', S., et al., Influence of humidity on the aerosol scattering coefficient and its effect on the upwelling radiance during ACE-2, *Tellus, Ser. B*, 52, 546–567, 2000.

- Goldsmith J. E. M., F.H. Blair, S.E. Bisson, and D.D. Turner, Turn-Key Raman lidar for profiling atmospheric water vapor, clouds, and aerosols. *Appl. Opt.*, 37, 4979–4990, 1998.
- Harder J. W., J. W. Brault, P. V. Johnston, and G. H. Mount, Temperature dependent NO<sub>2</sub> cross sections at high spectral resolution, *J. Geophys. Res.*, 102, 3861-3879, 1997.
- Hartley, W. S., P. V. Hobbs, J. L. Ross, P. B. Russell, and J. M. Livingston, Properties of aerosols aloft relevant to direct radiative forcing off the mid-Atlantic coast of the United States, *J. Geophys. Res.*, 105, 9859–9885, 2000.
- Haywood, J.M., and V. Ramaswamy, Global sensitivity studies of the direct radiative forcing due to anthropogenic sulfate and black carbon aerosols, *J. Geophys. Res.*, 103, 6043-6058, 1998.
- Hegg, D.A., J. Livingston, P.V. Hobbs, T. Novakov, and P. Russell, Chemical apportionment of aerosol column optical depth off the mid-Atlantic coast of the United States, *J. Geophys. Res.*, 102,25,293–25,303, 1997.
- Jaffe, D., I. Bertschi, L. Jaegle', P. Novelli, J. S. Reid, H. Tanimoto, R. Vingarzan, and D. L. Westphal, Long-range transport of Siberian biomass burning emissions and impact on surface ozone in western North America. *Geophys. Res. Lett.*, 31, doi:10.1029/2004GL020093, 2004.
- Kasten, F., Visibility in the phase of pre-condensation, *Tellus*, 21, 631–635, 1969.
- Kato, S., et al., A comparison of the aerosol thickness derived from ground-based and airborne measurements, *J. Geophys. Res.*, 105, 14,701–14,717, 2000.

- Liljegren, J., S.A. Boukabara, K. Cody-Pereira, and S.A. Clough, The effect of the half-width of the 22 GHz water vapor line on retrievals of temperature and water vapor profiles with a twelve-channel microwave radiometer, *IEEE Trans. Geoscience Remote Sensing*, in press, 2004.
- Linné, H., D.D. Turner, J.E.M. Goldsmith, T.P. Tooman, J. Bösenberg, K. Ertel, and S. Lehmann, Intercomparison of DIAL and RAMAN lidar measurements of humidity profiles. *Advances in Laser Remote Sensing: Selected Papers Presented at the 20th International Laser Radar Conference*, D. Dabas, C. Loth, and J. Pelon, Eds., Ecole Polytechnique, 293 –298, 2001.
- Masonis, S.J, K. Franke, A. Ansmann, D. Muller, D. Althausen, J.A. Ogren, A. Jefferson, P. J. Sheridan, An intercomparison of aerosol light extinction and 180° backscatter as derived using *in situ* instruments and Raman lidar during the INDOEX field campaign, *J. Geophys. Res.*, 107, No. D19, 8014, doi:10.1029/2000JD000035, 2002
- Matsumoto, T., P. B. Russell, C. Mina, W. Van Ark and V. Banta, Airborne Tracking Sunphotometer. *J. Atmos. Ocean. Tech.*, Vol. 4, 336-339, 1987.
- Mattis et al., “Siberian Forest-Fire Smoke Observed over Central Europe in Spring/Summer 2003 in the Framework of EARLINET”, 22<sup>nd</sup> International Laser Radar Conference, G. Pappalardo and A. Amodeo, eds., pp. 857-860, 2004.
- Murayama et al., “Optical Characteristics of Dust and Smoke Aerosols Observed with Multi-wavelength Raman Lidar in Tokyo”, 22<sup>nd</sup> International Laser Radar Conference, G. Pappalardo and A. Amodeo, eds., pp. 365-368, 2004.
- Nash, J., T. J. Oakley, and C. Gaffard, Progress in improving upper air moisture measurements over the UK. Preprints, *12th Symp. on Meteorological Observations and Instrumentation*, Long Beach, CA, Amer. Meteor. Soc., 8.5, 2003.



- Redemann, J., R.P. Turco, K.N. Liou, P.B. Russell, R.W. Bergstrom, B. Schmid, J.M. Livingston, P.V. Hobbs, W.S. Hartley, S. Ismail, R.A. Ferrare, E.V. Browell, Retrieving the vertical structure of the effective aerosol complex index of refraction from a combination of aerosol *in situ* and remote sensing measurements during TARFOX, *J. Geophys. Res.*, *105*, 9949-9970, 2000.
- Redemann, J., P. B. Russell, and P. Hamill, Dependence of aerosol light absorption and single-scattering albedo on ambient relative humidity for sulfate aerosols with black carbon cores, *J. Geophys. Res.*, *106*, 27,485 – 27,495, 2001.
- Revercomb H., D.D. Turner, D.C. Tobin, R.O. Knuteson, W.F. Feltz, B. Balsley, J. Barnard, J. Bösenberg, S. Clough, D. Cook, R. Ferrare, J. Goldsmith, S. Gutman, R. Halthore, B. Lesht, J. Liljegren, H. Linné, J. Michalsky, V. Morris, W. Porch, S. Richardson, B. Schmid, M. Splitt, T. Van Hove, E. Westwater, and D. Whiteman, The Atmospheric Radiation Measurement (ARM) Program's Water Vapor Intensive Observation Periods, *Bull. Amer. Meteor. Soc.*, *84*, 217-236, 2003.
- Rosenkranz, P., Water vapor continuum absorption: a comparison of measurements and models. *Radio Sci*, *33*, 919-928, 1998.
- Rothman L.S., K. Chance, J. Schroeder, and A. Goldman. New Edition of HITRAN Database. 11<sup>th</sup> ARM Science Team Meeting Proceedings, Atlanta, Georgia, March 19-23, 2001.
- Rothman L.S., and J. Schroeder, Millenium HITRAN Compilation. 12<sup>th</sup> ARM Science Team Meeting Proceedings, St. Petersburg, Florida, April 8-12, 2002.
- Ruggaber, A., R. Dlugi, and T. Nakajima, Modelling radiation quantities and photolysis frequencies in the troposphere, *J. Atmos. Chem.*, **18**, 171-210, 1994.

Russell, P. B., J. M. Livingston, E. G. Dutton, R. F. Pueschel, J. A. Reagan, T. E. Defoor, M. A. Box, D. Allen, P. Pilewskie, B. M. Herman, S. A. Kinne, and D. J. Hofmann, Pinatubo and pre-Pinatubo optical-depth spectra: Mauna Loa measurements, comparisons, inferred particle size distributions, radiative effects, and relationship to lidar data. *J. Geophys. Res.*, *98*, 22'969-22'985, 1993.

Russell, P.B. et al., Comparison of Aerosol Single Scattering Albedos Derived by Diverse Techniques in Two North Atlantic Experiments, *Journal of the Atmospheric Sciences*: Vol. 59, No. 3, pp. 609–619, 2002.

Schmid, B., and C. Wehrli, Comparison of sun photometer calibration by Langley technique and standard lamp, *Appl. Opt.*, *34*, 4500-4512, 1995.

Schmid, B., P. R. Spyak, S. F. Biggar, C. Wehrli, J. Sekler, T. Ingold, C. Mätzler, and N. Kämpfer, Evaluation of the applicability of solar and lamp radiometric calibrations of a precision Sun photometer operating between 300 and 1025 nm, *Appl. Opt.*, *37*, 3923-3941, 1998.

Schmid, B., J. M. Livingston, P. B. Russell, P. A. Durkee, H. H. Jonsson, D. R. Collins, R. C. Flagan, J. H. Seinfeld, S. Gassó, D. A. Hegg, E. Öström, K. J. Noone, E. J. Welton, K. J. Voss, H. R. Gordon, P. Formenti, and M. O. Andreae, Clear sky closure studies of lower tropospheric aerosol and water vapor during ACE 2 using airborne sunphotometer, airborne in-situ, space-borne, and ground-based measurements, *Tellus*, B *52*, 568-593, 2000.

Schmid B., J. J. Michalsky, D. W. Slater, J. C. Barnard, R. N. Halthore, J. C. Liljegren, B. N. Holben, T. F. Eck, J. M. Livingston, P. B. Russell, T. Ingold, and I. Slutsker, Comparison of columnar water-vapor measurements from solar transmittance methods. *Appl. Opt.*, *40*, 1886-1896, 2001.

- Schmid B., J. Redemann, P. B. Russell, P. V. Hobbs, D. L. Hlavka, M. J. McGill, B. N. Holben, E. J. Welton, J. R. Campbell, O. Torres, R. A. Kahn, D. J. Diner, M. C. Helmlinger, D. A. Chu, C. Robles Gonzalez, and G. de Leeuw, Coordinated airborne, spaceborne, and ground-based measurements of massive, thick aerosol layers during the dry season in southern Africa, *J. Geophys. Res.*, 108(D13), 8496, doi:10.1029/2002JD002297, 2003a.
- Schmid B., D. A. Hegg, J. Wang, D. Bates, J. Redemann, P. B. Russell, J. M. Livingston, H. H. Jonsson, E. J. Welton, J. H. Seinfeld, R. C. Flagan, D. S. Covert, O. Dubovik, and A. Jefferson. Column closure studies of lower tropospheric aerosol and water vapor during ACE-Asia using airborne sunphotometer, airborne in-situ and ship-based lidar measurements. *J. Geophys. Res.*, 108(D23), 8656, doi:10.1029/2002JD003361, 2003b.
- Schmid, B., D. Covert, J. Eilers, R. Elleman, R. Ferrare, C. Flynn, B. Holben, H. Jonsson, J. Redemann, K. Ricci, A. Strawa, D. Turner, E. Welton, Column Closure studies of tropospheric aerosol and water vapor during the May 2003 ARM Aerosol IOP, submitted to *J. Geophys. Res.*, 2005.
- Sheridan, P.J. , D. J. Delene, and J. A. Ogren, 2001: Four years of continuous surface aerosol measurements from the Department of Energy's Atmospheric Radiation Measurement Program Southern Great Plains Cloud and Radiation Testbed site. *J. Geophys. Res.*, **106**, 20 735–20 747.
- Sheridan, P. J., A. Jefferson, and J. A. Ogren (2002), Spatial variability of submicrometer aerosol radiative properties over the Indian Ocean during INDOEX, *J. Geophys. Res.*, 107(D19), 8011, doi:10.1029/ 2000JD000166.
- Turner, D.D., and J.E.M. Goldsmith, Twenty-Four hour Raman lidar measurements during the Atmospheric Radiation Measurement program's 1996 and 1997 water vapor intensive observation periods. *J. Atmos. Oceanic Technol.*, **16**, 1062-1076, 1999.

- Turner, D.D., H. Linné, J. Bösenberg, S. Lehmann, K. Ertel, J. E. M. Goldsmith and T. P. Tooman, Simultaneous Ground-Based Remote Sensing of Water Vapor by Differential Absorption and Raman Lidars, Tenth ARM Science Team Meeting Proceedings, San Antonio, Texas, March 13-17, 2000, <http://www.arm.gov/publications/proceedings/conf10/abstracts/turner-dd.pdf>
- Turner, D.D., R.A. Ferrare, and L.A. Brasseur, Average aerosol extinction and water vapor profiles over the Southern Great Plains. *Geophys. Res. Lett.*, 28, 4441-4444, 2001.
- Turner D.D., R.A. Ferrare, L.A. Heilman, W.F. Feltz, and T. Tooman, Automated Retrievals of Water Vapor and Aerosol Profiles over Oklahoma from an Operational Raman Lidar, *J. Atmos. Oceanic Tech.*, 19, 37-50, 2002.
- Turner, D.D., R.A. Ferrare, and M.B. Clayton, Summary of the processing of the aerosol data from the ARM Raman lidar for the 2003 ARM Aerosol IOP, [http://iop.archive.arm.gov/arm-iop-file/2003/sgp/aerosol/ferrare-raman/2003\\_aerosol\\_iop\\_summary.pdf](http://iop.archive.arm.gov/arm-iop-file/2003/sgp/aerosol/ferrare-raman/2003_aerosol_iop_summary.pdf), 2003a.
- Turner D.D., B.M. Lesht, S.A. Clough, J.C. Liljegren, H.E. Revercomb, and D.C. Tobin, Dry bias and variability in Vaisala RS80-H radiosondes: The ARM experience. *J. Atmos. Oceanic Technol.*, 20, 117–132, 2003b.
- Turner, D.D., K.L. Gaustad, S.A. Clough, K. Cady-Pereira, E.J. Mlawer, J.C. Liljegren, and E.E. Clothiaux, Improved PWV and LWP retrievals from the microwave radiometer for ARM. Proceedings of the 14th ARM Science Team Meeting, Albuquerque, NM. Available at [http://www.arm.gov/publications/proceedings/conf14/extended\\_abs/turner3-dd.pdf](http://www.arm.gov/publications/proceedings/conf14/extended_abs/turner3-dd.pdf), 2004.
- Vance, A. K., J.P. Taylor, T.J. Hewison, and J. Elms, 2004: Comparison of In Situ Humidity Data from Aircraft, Dropsonde, and Radiosonde, *J. Atmos. Oceanic Technol.*, 21, 921-932.

- Wandinger, U. and Ansmann, A. 2002. Experimental determination of the lidar overlap profile with Raman Lidar. *Appl. Opt.*, 41, 511-514.
- Wandinger et al., “Optical and microphysical characterization of biomass burning and industrial pollution aerosols from multiwavelength lidar and aircraft measurements”, *J. Geophys. Res.*, 107, doi:10.1029/2000JD000202, 2002.
- Wendisch, M., S. Mertes, A. Ruggaber, and T. Nakajima, Vertical Profiles of Aerosol and Radiation and the Influence of a Temperature Inversion: Measurements and Radiative Transfer Calculations, *J. Appl. Meteor.*, **35**, 1703-1715, 1996.
- Whiteman D.N., Examination of the traditional Raman lidar technique. II. Evaluating the ratios for water vapor and aerosols, *Appl. Opt.* 42, 2593–2608, 2003.
- Whiteman, D.N., K. D. Evans, B. Demoz, D. O’C. Starr, E. W. Eloranta, D. Tobin, W. Feltz, G. J. Jedlovec, S. I. Gutman, G. K. Schwemmer, M. Cadirola, S. H. Melfi, and F. J. Schmidlin, Raman lidar measurements of water vapor and cirrus clouds during the passage of Hurricane Bonnie, *J. Geophys. Res.*, 106, 5211–5225, 2001.
- Whiteman D. N., B. Demoz, Z. Wang, Subtropical cirrus cloud extinction to backscatter ratios measured by Raman Lidar during CAMEX-3, *Geophys. Res. Lett.*, 31, L12105, doi:10.1029/2004GL020003, 2004.
- Whiteman, D.N., B. Demoz, P. Di Girolamo, J. Comer, I. Veselovskii, K. Evans, Z. Wang, M. Cadirola, K. Rush, D. Sabatino, G. Schwemmer, B. Gentry, S. H. Melfi, B. Mielke, T. VanHove, E. Browell, R. Ferrare, J. Wang, Raman Water Vapor Lidar Measurements During the International H<sub>2</sub>O Project - Improved Measurement Capability, to be submitted to *J. Atmos. Oceanic Tech.*, 2005.

Table 1. May 2003 Aerosol IOP water vapor comparison results

	Least Squares Regression				N	D <sup>#</sup>	C <sup>##</sup>	Bias Difference* (g/m <sup>3</sup> ) (%)	RMS Difference (g/m <sup>3</sup> ) (%)
	Bisector Slope	Intercept (g/m <sup>3</sup> )	Standard Linear Slope	Intercept (g/m <sup>3</sup> )					
Radiosonde (day)	0.89	0.23	0.85	0.45	2002	22	35	-0.48 (-7.6%)	1.1 (18%)
MWR-scaled radiosonde (day)	0.95	0.32	0.91	0.56	2002	22	35	0.0097 (0.15%)	1.0 (16%)
Radiosonde (night)	0.93	0.092	0.91	0.22	1650	17	24	-0.27 (-5.0%)	0.76 (14%)
MWR-scaled radiosonde (night)	0.96	0.067	0.93	0.20	1650	17	24	-0.17 (-3.1%)	0.72 (13%)
AATS14	0.91	-0.077	0.87	0.14	786	12	21	-0.65 (-11%)	1.2 (21%)
Chilled mirror	0.87	0.21	0.84	0.40	786	12	21	-0.59 (-10%)	1.2 (21%)
IAP	0.87	-0.34	0.86	-0.27	69	10	10	-1.25 (-17%)	1.5 (20%)

\* difference = sensor - CARL

D<sup>#</sup> = number of days

C<sup>##</sup> = number of profiles compared

Table 2. May 2003 Aerosol IOP aerosol extinction comparison results

	Least Squares Regression				N	D <sup>#</sup>	C <sup>##</sup>	Bias Difference* (km <sup>-1</sup> ) (%)	RMS Difference (km <sup>-1</sup> ) (%)	
	Bisector Slope	Intercept (km <sup>-1</sup> )	Standard Linear Slope	Intercept (km <sup>-1</sup> )						R
AATS14 (354 nm)	0.92	-0.020	0.74	-0.0056	0.81	537	8	14	-0.026 (-33%)	0.048 (61%)
Twin Otter (neph+PSAP) (450 nm)	0.70	-0.012	0.51	-0.00034	0.74	759	12	25	-0.031 (-50%)	0.049 (78%)
IAP (neph+PSAP) (450 nm)	0.76	-0.012	0.62	-0.00094	0.82	65	9	9	-0.032 (-40%)	0.051 (64%)

\* difference = sensor - CARL

D<sup>#</sup> = number of days

C<sup>##</sup> = number of profiles compared

Table 3. May 2003 Aerosol IOP aerosol extinction comparison results (450 nm)

Date	Time (UT)	Altitude (km)	$\omega_o$ (retrieved)	$\omega_o$ (measured)*	Refractive index	
					Real	Imaginary
May 17	22:10	0.7	0.98 (0.03)	0.97 (0.02)	1.41 (0.02)	0.001 (0.002)
May 18	17:00	0.5	0.94 (0.04)	0.97 (0.02)	1.45 (0.03)	0.005 (0.004)
May 22	14:50	0.5	0.95 (0.03)	0.96 (0.02)	1.45 (0.04)	0.003 (0.003)
May 25	21:40	3.0	0.98 (0.02)	0.96 (0.02)	1.55 (0.03)	0.003 (0.002)
May 25	20:30	0.8	0.98 (0.02)	0.96 (0.02)	1.50 (0.04)	0.002 (0.003)
May 27	17:30	3.5	0.91 (0.05)	0.95 (0.02)	1.60 (0.03)	0.009 (0.003)

\* Derived from Twin Otter *in situ* nephelometer measurements of aerosol scattering and PSAP measurements of absorption

## Figure Captions

Figure 1. (a) Random errors associated with the retrievals of the aerosol backscatter coefficient at an altitude of about 2 km. (b) same except for water vapor mixing ratio. (c) Maximum altitudes of the water vapor mixing ratio retrievals. Daytime retrievals denoted by (+) and nighttime retrievals are denoted by (•). Three day running mean averages are shown in red for daytime retrievals and in blue for nighttime retrievals.

Figure 2. (a) Comparison of water vapor profiles acquired on May 22 during the IOP. (b) same except for aerosol extinction. Error bars represent the standard deviations of the measurements during the averaging period. Times shown are UT hours.

Figure 3. Comparison of water vapor profiles derived by CARL (blue), AATS14 airborne Sun photometer (red), and airborne *in situ* chilled mirror (green) instruments for various days in May 2003 during the IOP. Error bars represent the standard deviations of the measurements during the averaging period.

Figure 4. (a) Regression comparison of CARL and MWR-scaled radiosonde daytime measurements of water vapor profiles during the IOP. (b) same except for CARL and the chilled mirror sensor on the Twin Otter.

Figure 5. Average bias differences between the CARL water vapor measurements and the various other measurements for water vapor values between 0 and 3 km. Error bars represent the standard deviation of the measurements.

Figure 6. (a) Water vapor profiles derived from CARL, unscaled and MWR-scaled Vaisala RS90 radiosonde, and chilled mirror measurements between 17:00-19:00 UT on May 17. (b) same except for relative humidity. Cloud base height derived from the lidar and *in situ* aircraft measurements is indicated by the dashed line.



Figure 7. Comparison of aerosol extinction profiles (450 nm) derived by CARL (blue), AATS-14 airborne Sun photometer (red), and airborne nephelometer+PSAP (green) Twin Otter instruments for various days in May 2003 during the IOP. Error bars represent the standard deviations of the measurements during the averaging period for the CARL and nephelometer+PSAP measurements. The error bars for the AATS-14 results represent uncertainty estimates of these measurements.

Figure 8. (a) Regression comparison of aerosol extinction values (354 nm) derived from CARL and AATS-14 Sun photometer measurements during the IOP. (b) same except for CARL and the aerosol extinction values (450 nm) derived from *in situ* measurements of aerosol scattering (nephelometer) and absorption (PSAP) on the Twin Otter. The CARL measurements of aerosol extinction were extrapolated to 450 nm using the Ångström exponent derived from the *in situ* measurements (450-700 nm).

Figure 9. Average bias differences between aerosol extinction (354 nm) derived from the CARL and AATS14 measurements.

Figure 10. Aerosol extinction profiles derived from Raman lidar (CARL), airborne Sun photometer (AATS14), and *in situ* (neph+PSAP) measurements acquired on May 25, 2003 over the ARM SGP site. Measured ( $S_a$ , AOT,  $\hat{a}$ ,  $r_{eff}$ ,  $\omega_o$ ) and derived ( $\omega_o$ ,  $m_r$ ,  $m_i$ ) aerosol properties for smoke and boundary layer aerosols are also shown.

Figure 11. (A) CARL water vapor mixing ratio profiles for September 25, 1998. (B) same except for September 26, 2004. (C) CARL water vapor mixing ratio random errors (%) for September 25, 1998. (D) same except for September 26, 2004. (E) CARL aerosol scattering profiles measured on September 25, 1998. (F) same except for September 26, 2004. (G) CARL aerosol scattering ratio random errors (%) for September 26, 2004. The images on the left represent examples of CARL measurements during the first year of routine CARL operations. The images on the right represent examples of CARL measurements after extensive modifications to the

system in 2004. Nighttime measurements occurred between about 0000 UT and 1230 UT; daytime measurements occurred between about 1230 UT and 0000 UT.

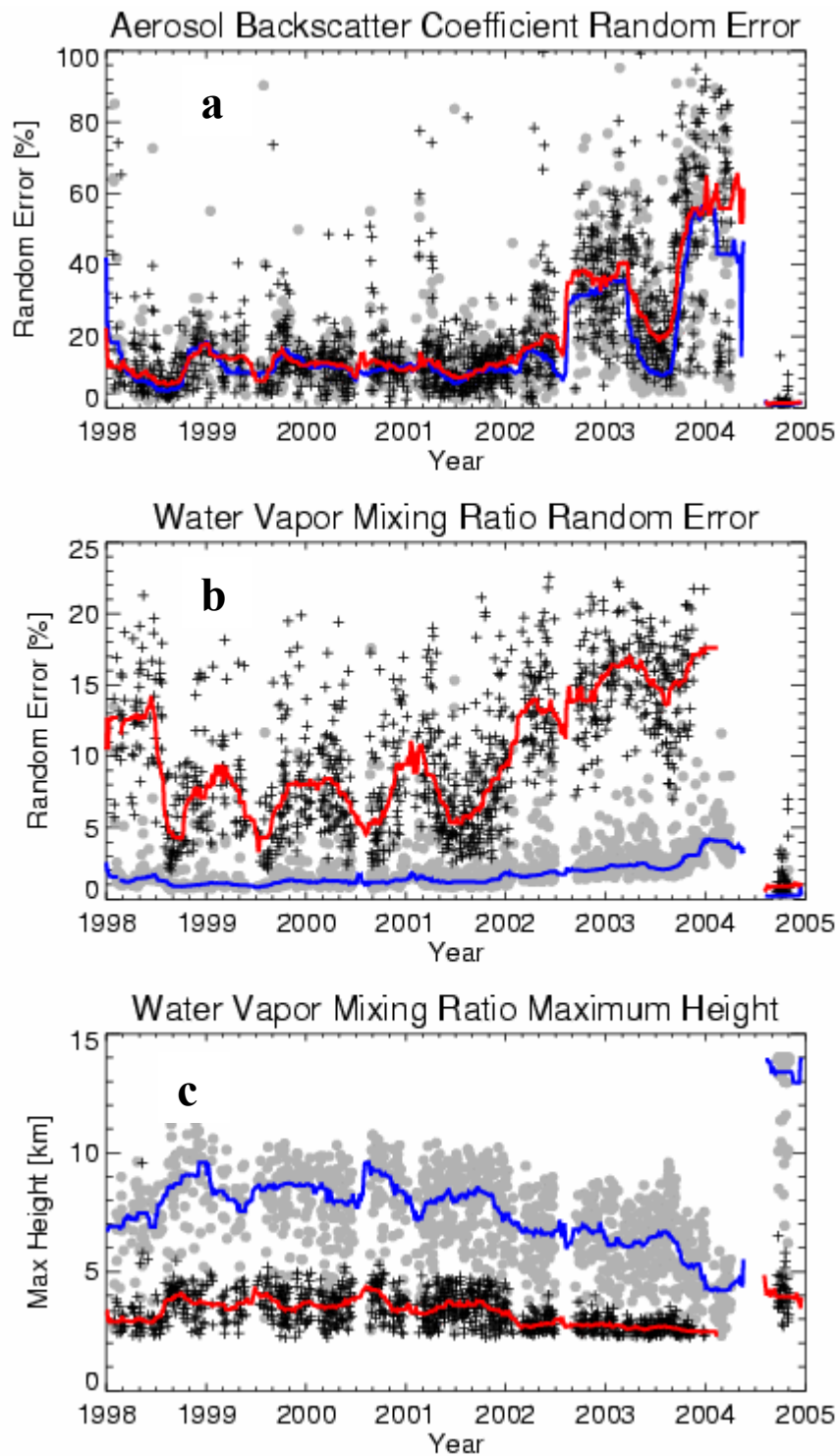


Figure 1. (a) Random errors associated with the retrievals of the aerosol backscatter coefficient at an altitude of about 2 km. (b) same except for water vapor mixing ratio. (c) Maximum altitudes of the water vapor mixing ratio retrievals. Daytime retrievals denoted by (+) and nighttime retrievals are denoted by (•). Three day running mean averages are shown in red for daytime retrievals and in blue for nighttime retrievals.

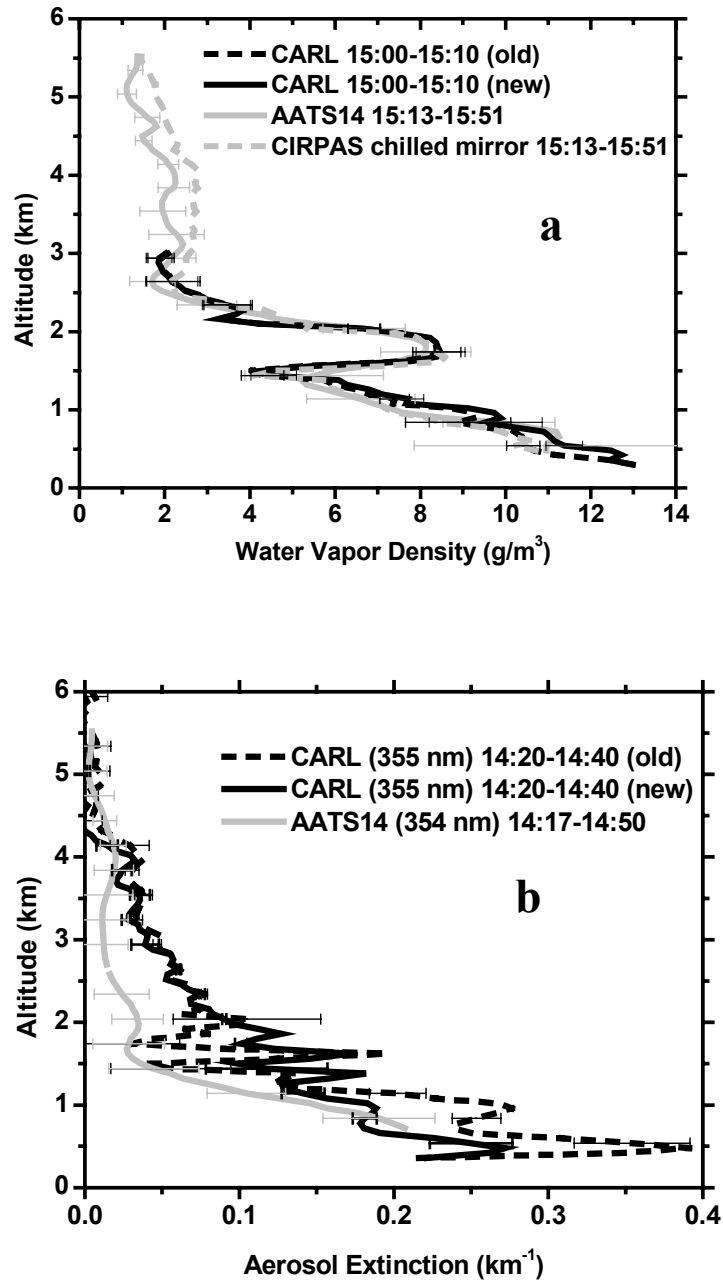


Figure 2. (a) Comparison of water vapor profiles acquired on May 22 during the IOP. (b) same except for aerosol extinction. Error bars represent the standard deviations of the measurements during the averaging period. Times shown are UT hours.

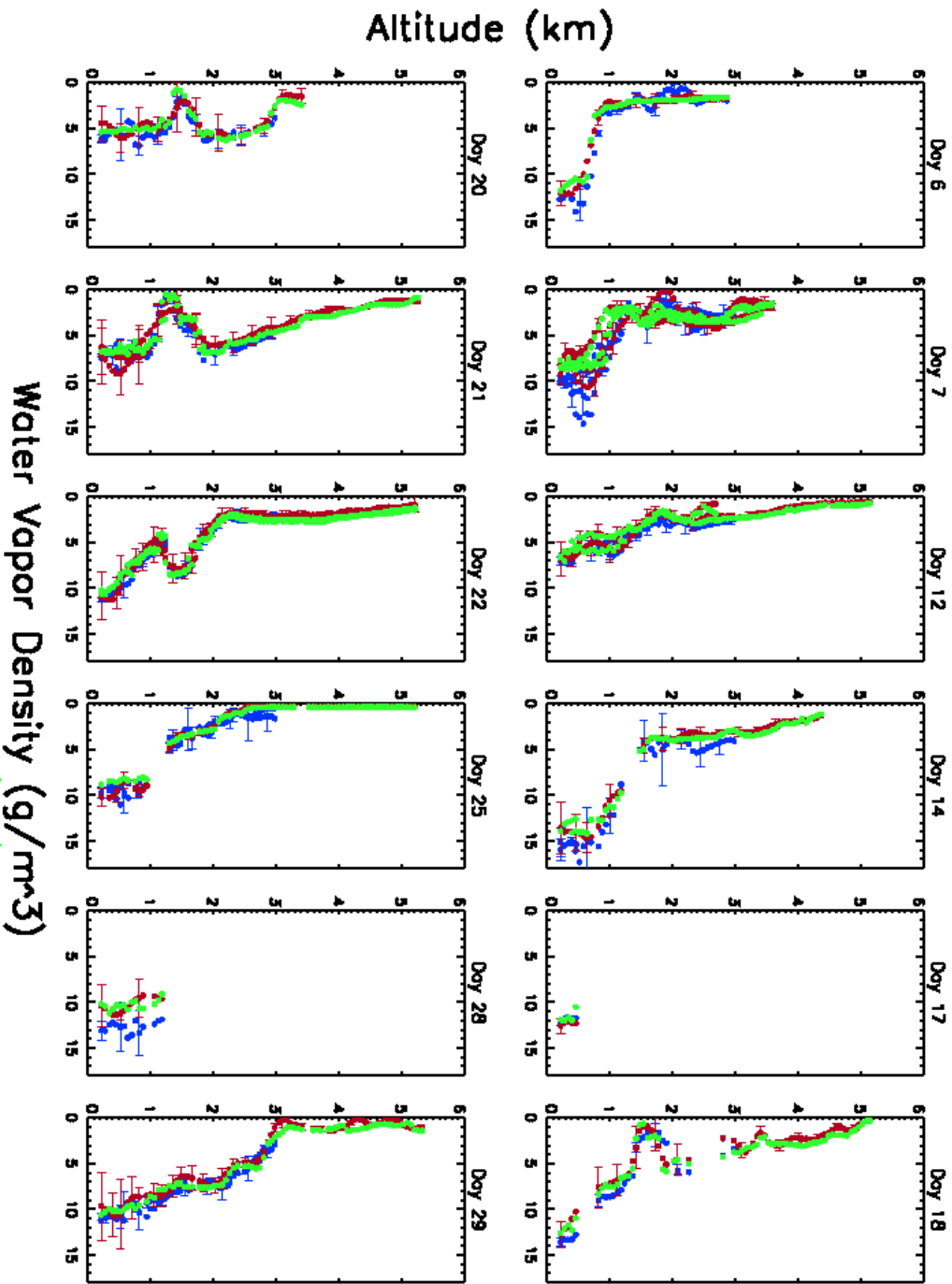


Figure 3. Comparison of water vapor profiles derived by CARL (blue), AATS14 airborne Sun photometer (red), and airborne in situ chilled mirror (green) instruments for various days in May 2003 during the IOP. Error bars represent the standard deviations of the measurements during the averaging period.

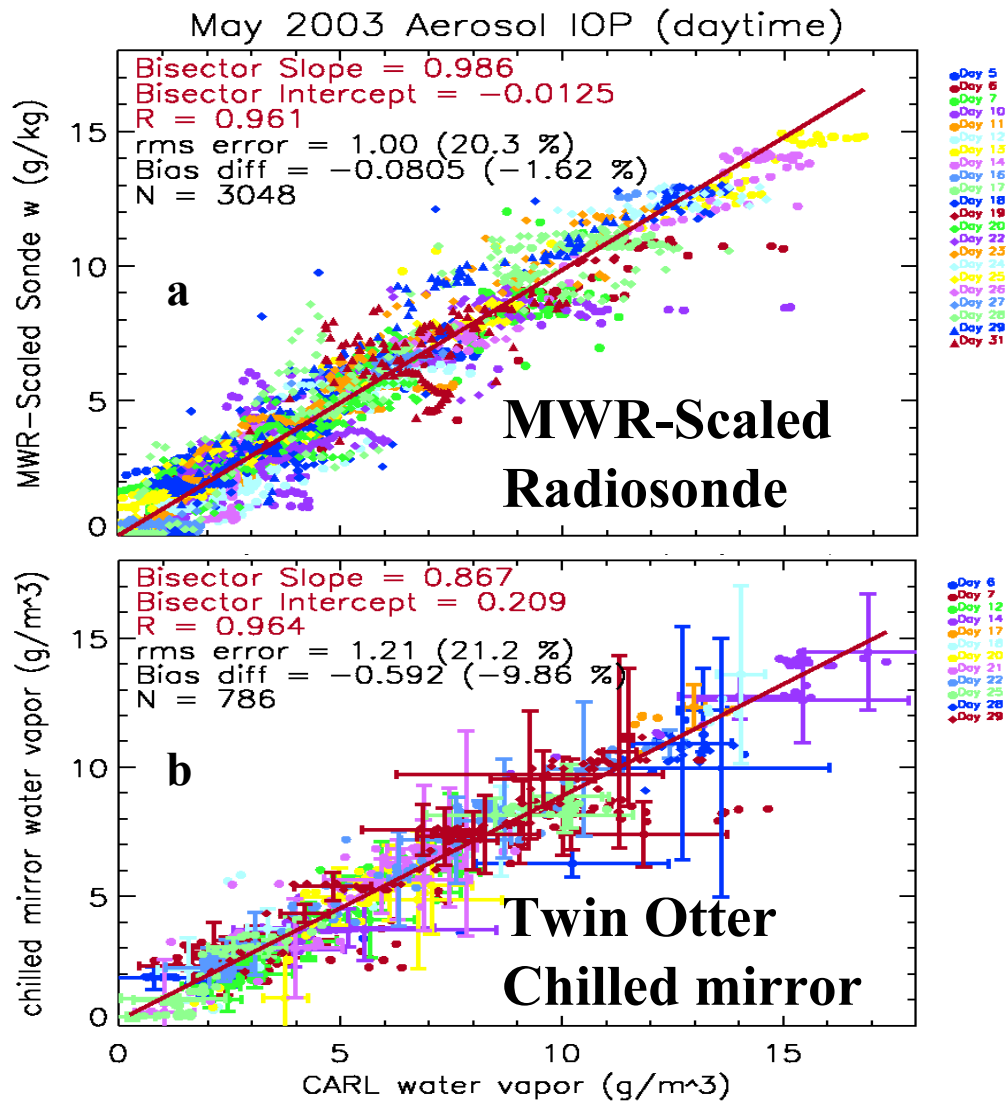


Figure 4. (a) Regression comparison of CARL and MWR-scaled radiosonde daytime measurements of water vapor profiles during the IOP. (b) same except for CARL and the chilled mirror sensor on the Twin Otter.

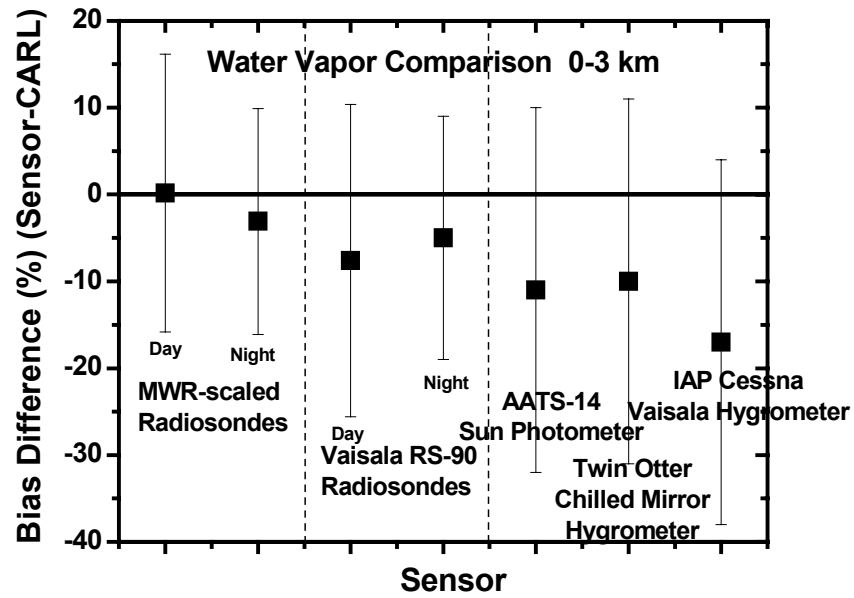


Figure 5. Average bias differences between the CARL water vapor measurements and the various other measurements for water vapor values between 0 and 3 km. Error bars represent the standard deviation of the measurements.

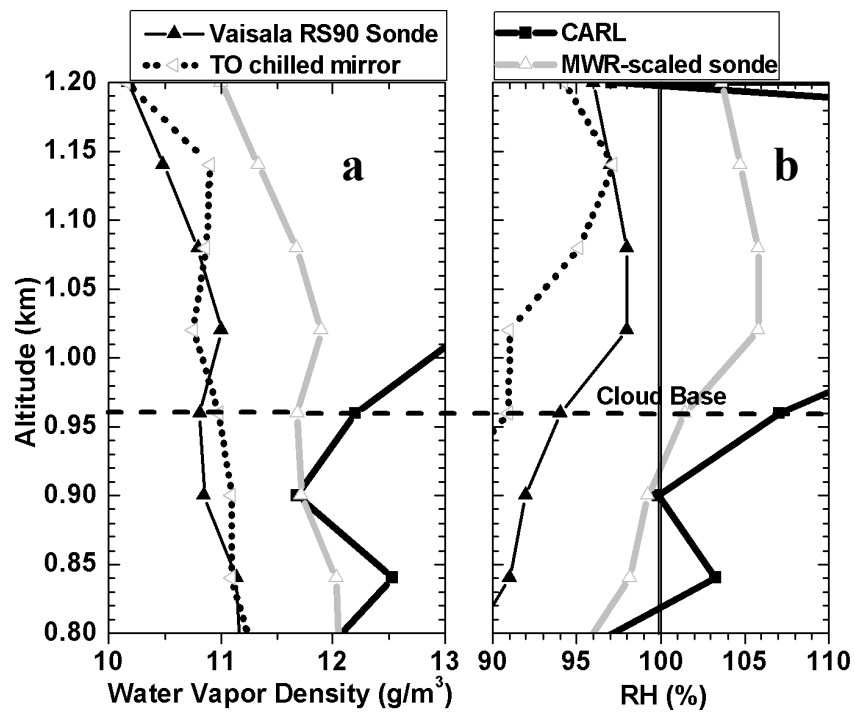


Figure 6. (a) Water vapor profiles derived from CARL, unscaled and MWR-scaled Vaisala RS90 radiosonde, and chilled mirror measurements between 17:00-19:00 UT on May 17. (b) same except for relative humidity. Cloud base height derived from the lidar and in situ aircraft measurements is indicated by the dashed line.



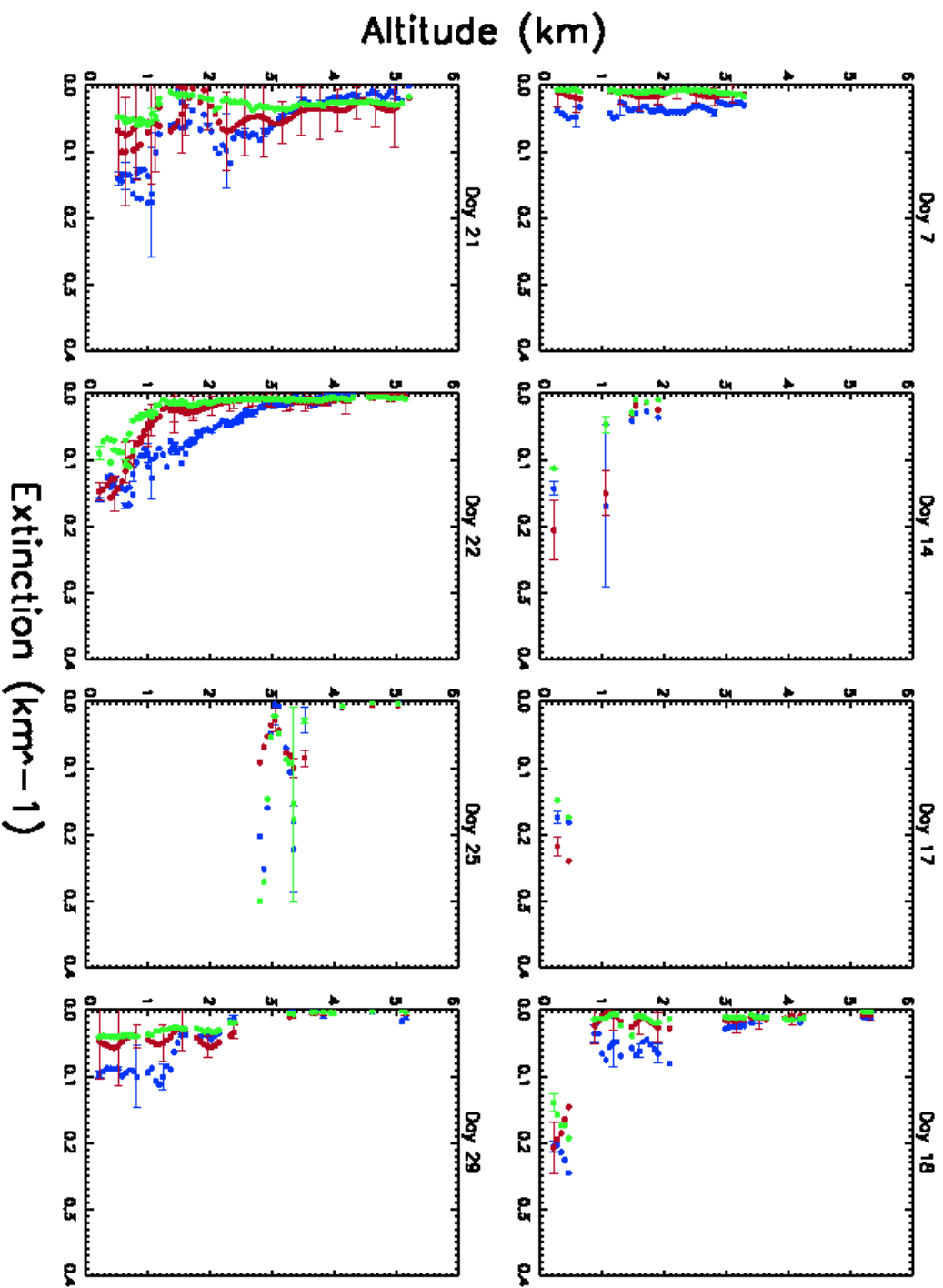


Figure 7. Comparison of aerosol extinction (450 nm) profiles derived by CARL (blue), AATS14 airborne Sun photometer (red), and airborne nephelometer+PSAP (green) Twin Otter instruments for various days in May 2003 during the IOP. Error bars represent the standard deviations of the measurements during the averaging period for the CARL and nephelometer+PSAP measurements. The error bars for the AATS-14 results represent uncertainty estimates of these measurements.

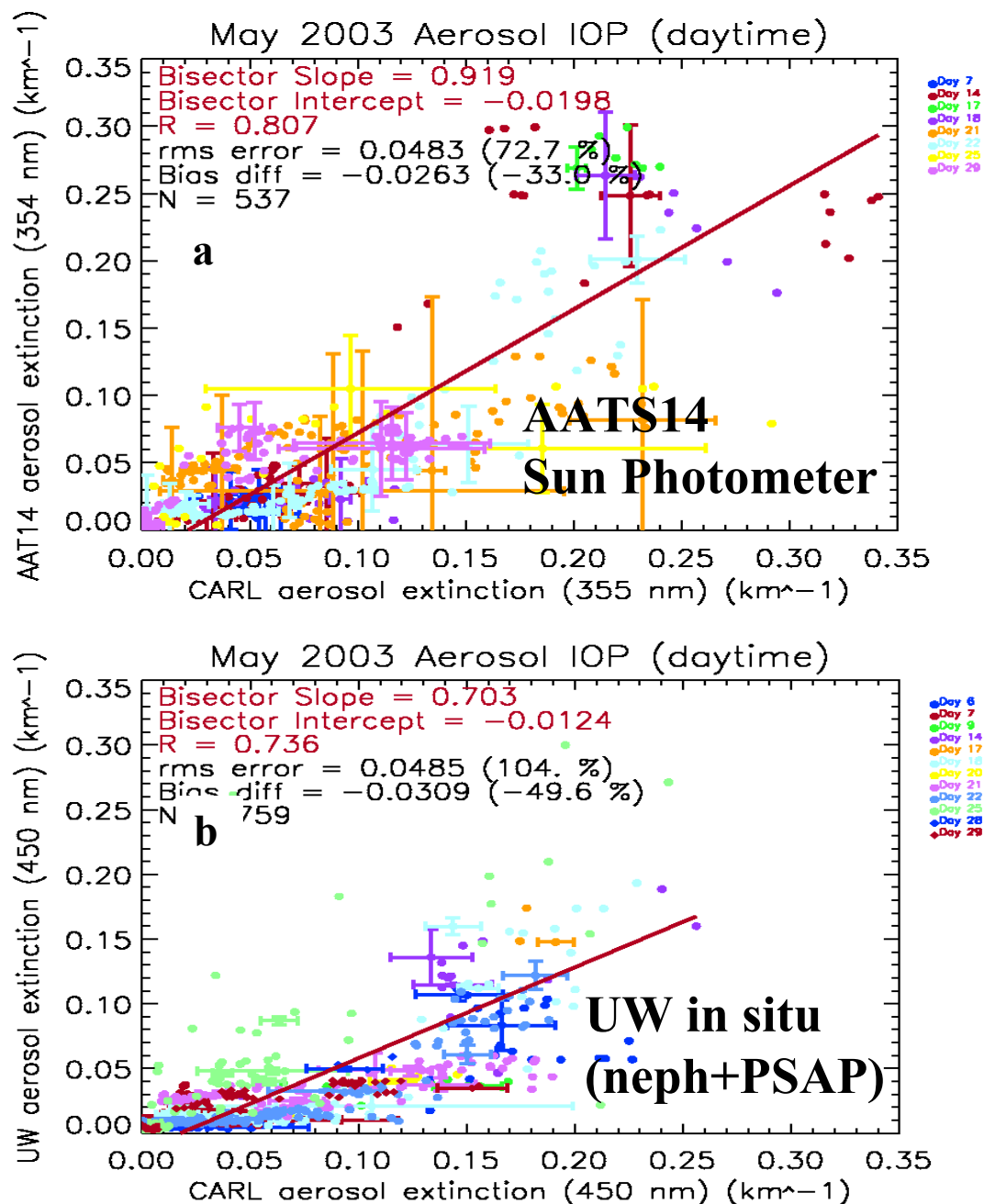


Figure 8. (a) Regression comparison of aerosol extinction values (354 nm) derived from CARL and AATS-14 Sun photometer measurements during the IOP. (b) same except for CARL and the aerosol extinction values (450 nm) derived from in situ measurements of aerosol scattering (nephelometer) and absorption (PSAP) on the Twin Otter. The CARL measurements of aerosol extinction were extrapolated to 450 nm using the Ångström exponent derived from the in situ measurements (450-700 nm).

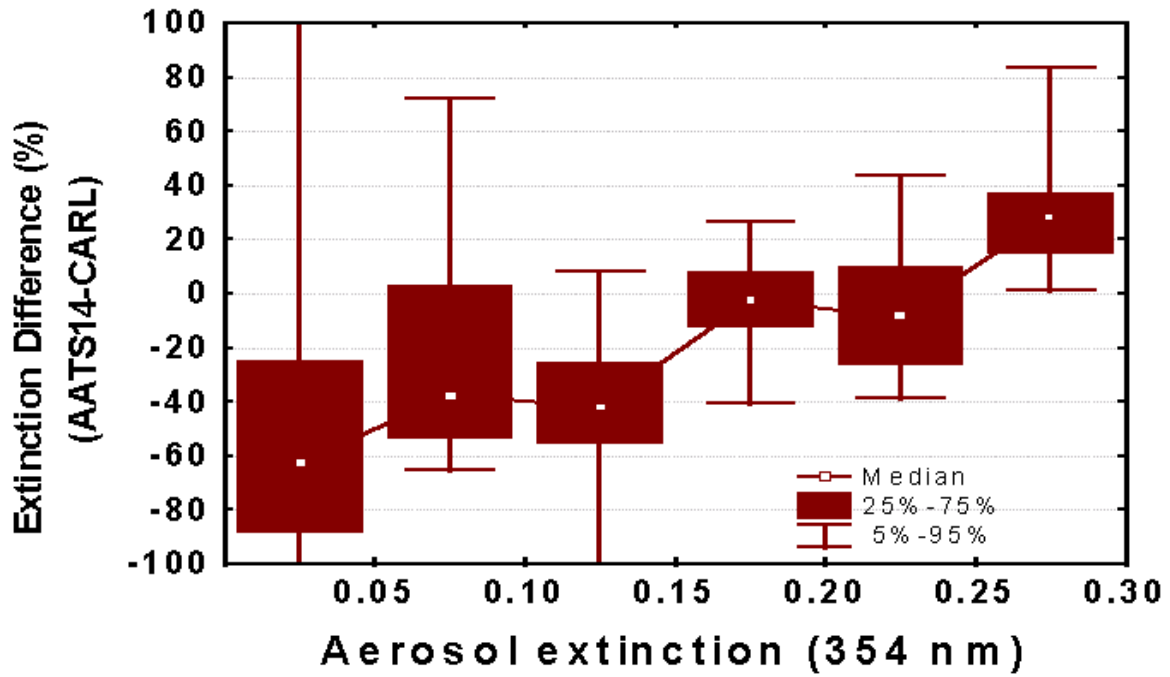


Figure 9. Average bias differences between aerosol extinction (354 nm) derived from the CARL and AATS14 measurements.

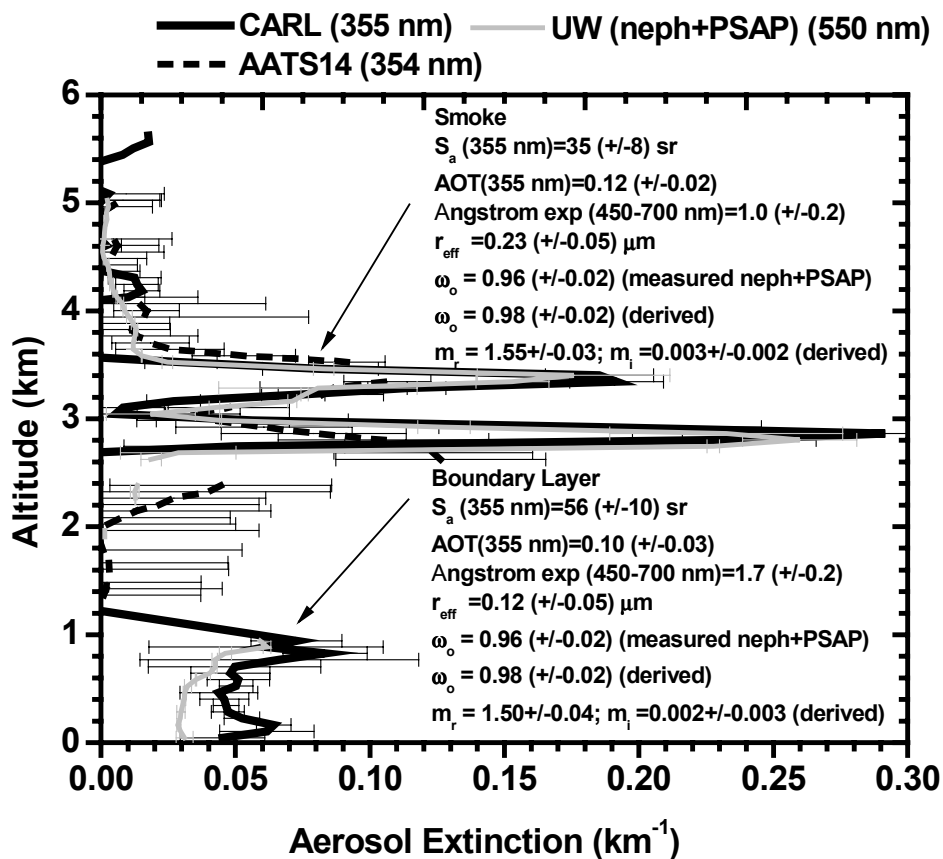


Fig. 10. Aerosol extinction profiles derived from Raman lidar (CARL), airborne Sun photometer (AATS14), and in situ (neph+PSAP) measurements acquired on May 25, 2003 over the ARM SGP site. Measured ( $S_a$ , AOT,  $\tilde{A}$ ,  $r_{eff}$ ,  $\omega_o$ ) and derived ( $\omega_o$ ,  $m_r$ ,  $m_i$ ) aerosol properties for smoke and boundary layer aerosols are also shown.

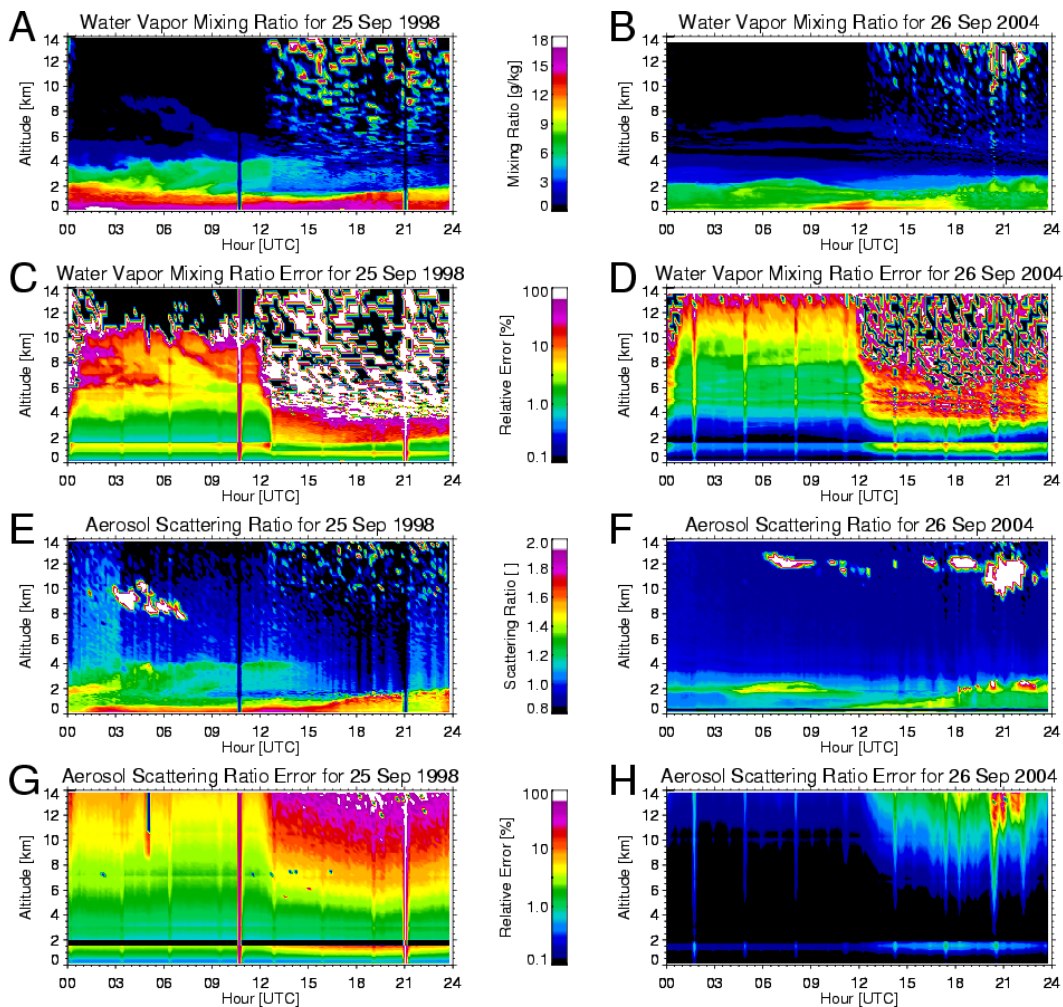


Figure 11. (A) CARL water vapor mixing ratio profiles for September 25, 1998. (B) same except for September 26, 2004. (C) CARL water vapor mixing ratio random errors (%) for September 25, 1998. (D) same except for September 26, 2004. (E) CARL aerosol scattering profiles measured on September 25, 1998. (F) same except for September 26, 2004. (G) CARL aerosol scattering ratio random errors (%) for September 26, 2004. The images on the left represent examples of CARL measurements during the first year of routine CARL operations. The images on the right represent examples of CARL measurements after extensive modifications to the system in 2004. Nighttime measurements occurred between about 0000 UT and 1230 UT; daytime measurements occurred between about 1230 UT and 0000 UT.